Redox Biology 46 (2021) 102127

Contents lists available at ScienceDirect

Redox Biology

journal homepage: www.elsevier.com/locate/redox

Genetic screening reveals phospholipid metabolism as a key regulator of the biosynthesis of the redox-active lipid coenzyme Q

Anita Ayer [a,b], Daniel J. Fazakerley [c,d], Cacang Suarna [a,b], Ghassan J. Maghzal [b], Diba Sheipouri [b], Kevin J. Lee [b], Michelle C. Bradley [e], Lucía Fernández-del-Rio [e], Sergey Tumanov [a,b], Stephanie MY. Kong [a,b], Jelske N. van der Veen [f], Andrian Yang [b,g], Joshua W.K. Ho [b,g,h,i], Steven G. Clarke [e], David E. James [c], Ian W. Dawes [j], Dennis E. Vance [k], Catherine F. Clarke [e], René L. Jacobs [f], Roland Stocker [a,b,g,l,*]

[a] Heart Research Institute, The University of Sydney, Sydney, New South Wales, Australia
[b] Victor Chang Cardiac Research Institute, Sydney, Australia
[c] Charles Perkins Centre, School of Life and Environmental Sciences, Sydney Medical School, The University of Sydney, Sydney, Australia
[d] Metabolic Research Laboratory, Wellcome-Medical Research Council Institute of Metabolic Science, University of Cambridge, Cambridge, United Kingdom
[e] Department of Chemistry and Biochemistry, and the Molecular Biology Institute, University of California, Los Angeles, United States
[f] Department of Agricultural, Food and Nutritional Science, University of Alberta, Edmonton, Canada
[g] St Vincent's Clinical School, University of New South Wales, Sydney, Australia
[h] School of Biomedical Sciences, Li Ka Shing Faculty of Medicine, University of Hong Kong, Hong Kong SAR, China
[i] Laboratory for Data Discovery for Health, Hong Kong Science Park, Hong Kong SAR, China
[j] School of Biotechnology and Biomolecular Sciences, University of New South Wales, Sydney, Australia
[k] Department of Biochemistry, University of Alberta, Edmonton, Canada
[l] School of Life and Environmental Sciences, The University of Sydney, Sydney, Australia

ARTICLE INFO

Keywords:
Coenzyme Q
Mitochondria
PEMT
Insulin resistance
S-adenosylmethionine
S-adenosylhomocysteine
Reactive oxygen species

ABSTRACT

Mitochondrial energy production and function rely on optimal concentrations of the essential redox-active lipid, coenzyme Q (CoQ). CoQ deficiency results in mitochondrial dysfunction associated with increased mitochondrial oxidative stress and a range of pathologies. What drives CoQ deficiency in many of these pathologies is unknown, just as there currently is no effective therapeutic strategy to overcome CoQ deficiency in humans. To date, large-scale studies aimed at systematically interrogating endogenous systems that control CoQ biosynthesis and their potential utility to treat disease have not been carried out. Therefore, we developed a quantitative high-throughput method to determine CoQ concentrations in yeast cells. Applying this method to the Yeast Deletion Collection as a genome-wide screen, 30 genes not known previously to regulate cellular concentrations of CoQ were discovered. In combination with untargeted lipidomics and metabolomics, phosphatidylethanolamine *N*-methyltransferase (PEMT) deficiency was confirmed as a positive regulator of CoQ synthesis, the first identified to date. Mechanistically, PEMT deficiency alters mitochondrial concentrations of one-carbon metabolites, characterized by an increase in the *S*-adenosylmethionine to *S*-adenosylhomocysteine (SAM-to-SAH) ratio that reflects mitochondrial methylation capacity, drives CoQ synthesis, and is associated with a decrease in mitochondrial oxidative stress. The newly described regulatory pathway appears evolutionary conserved, as ablation of PEMT using antisense oligonucleotides increases mitochondrial CoQ in mouse-derived adipocytes that translates to improved glucose utilization by these cells, and protection of mice from high-fat diet-induced insulin resistance. Our studies reveal a previously unrecognized relationship between two spatially distinct lipid pathways with potential implications for the treatment of CoQ deficiencies, mitochondrial oxidative stress/dysfunction, and associated diseases.

* Corresponding author. Heart Research Institute, 7 Eliza St Newtown, 2042, Australia.
E-mail address: roland.stocker@hri.org.au (R. Stocker).

https://doi.org/10.1016/j.redox.2021.102127
Received 27 July 2021; Received in revised form 27 August 2021; Accepted 4 September 2021
Available online 8 September 2021

1. Introduction

Mitochondrial dysfunction is increasingly recognized as a central mediator of many common disorders, including cardiovascular and metabolic diseases via the key role mitochondria play in cellular energy homeostasis and oxidant production. One of the central determinants of mitochondrial function is ubiquinone (or coenzyme Q, CoQ), an essential, evolutionarily conserved, redox active lipid in aerobic organisms. CoQ is best known for its function in mitochondrial ATP production, antioxidant protection and cell survival. More recently, the role of mitochondrial CoQ has expanded to the regulation of ferroptosis [1,2] nitric oxide synthase [3] and the homeostasis of brown adipose tissue [4].

There are two forms of CoQ deficiency in humans, both resulting in mitochondrial dysfunction. Primary CoQ deficiency results from mutations in CoQ biosynthetic genes and presents as a genetically and clinically heterogenous disorder [5]. Secondary CoQ deficiency occurs without underlying genetic defects in CoQ biosynthesis, yet is strongly associated with aging, insulin resistance and cardiovascular diseases such as atherosclerosis, myopathy, and heart failure [6–11]. Preclinical studies have established that increasing tissue CoQ can decrease mitochondrial oxidant production, improve mitochondrial function, and can ameliorate disease. Unfortunately however, translating this knowledge into the clinic has remained challenging, principally due to our inability to effectively restore CoQ concentrations in most human tissues as a result of the low bioavailability of orally supplemented CoQ [12]. A better understanding of the endogenous systems that regulate tissue CoQ content beyond the biosynthetic genes may help overcome this current limitation and identify new strategies to enhance endogenous CoQ biosynthesis.

Although CoQ was discovered more than 60 years ago, our understanding of how cells regulate their CoQ content has remained limited to individual factors required for optimal CoQ synthesis [13–15]. To date, a systemic approach aimed at identifying networks important for the regulation of cellular CoQ concentrations beyond the mevalonate pathway has not been carried out. A likely reason for this is the technically challenging nature of high-throughput CoQ extraction and analysis. To overcome this current limitation, we developed a large-scale screening method to analyze and quantify cellular CoQ using high-performance liquid chromatography coupled with electrochemical detection (HPLC-ECD). Using this platform, we used the Yeast Deletion Collection to conduct a genome-wide genetic screen and identified 30 new potential CoQ-regulating genes. Of these, we focused on phosphatidylethanolamine *N*-methyltransferase (PEMT) that plays a key role in phospholipid metabolism. We observed that cells deficient in PEMT contain strikingly higher concentrations of mitochondrial CoQ in multiple biological systems. Using genetic manipulations, lipidomics, and untargeted and targeted metabolomics, we discovered a previously unrecognized link between endoplasmic reticulum/mitochondrial associated membrane PEMT activity, and the mitochondrial methylation activity required for CoQ synthesis. Finally, we identified increased mitochondrial CoQ as the molecular basis for how PEMT deficiency protects mice against insulin resistance.

2. Methods

2.1. Genome-wide screen of mutants with altered total CoQ_6 content

The homozygous diploid yeast knockout collection (BY4743; Euroscarf) was used to screen genes that affected total CoQ_6 content. The collection is housed in a series of 96-well plates kept frozen at −80 °C. Briefly, cells were inoculated from −80 °C stocks with 2.4 μL of defrosted culture inoculated into 96-well plates containing 195 μL media. Cells were grown for 2 d at 30 °C with shaking. After 2 d, 2.4 μL of pre-culture was inoculated into 96-well plates containing 195 μL fresh media and cells were grown for 18 h at 30 °C with shaking. After 18 h, the OD_{600} was measured (Pherastar 96-well plate spectrophotometer) and the plate centrifuged (1500×*g*; 4 °C; 5 min) to pellet cells. 190 μL of supernatant was removed from each well and the cell pellet in each well resuspended in 50 μL of 155 mM ammonium acetate. The 96-well plate was frozen at −20 °C until CoQ_6 extraction and analysis. On the day of analysis, plates were defrosted and 50 μL of cell suspension was transferred to a glass-coated 96 deep-well plate containing 50 μL of glass beads per well. As a control, a separate batch of WT cells grown to OD_{600} ~1.0 and frozen in aliquots were used as quality control (QC) samples in each plate. Wells A1, E6 and H12 of each plate were used for the QC samples with 50 μL of QC sample put in each well on the day of analysis. For each plate to pass 'QC', the CoQ_6 content of the QC wells had to be within 20% of each other. Cells were lysed and CoQ_6 extracted and analyzed as outlined below.

2.2. Determination of CoQ_6 and ergosterol content in yeast cells

The method used was adapted from Gay & Stocker 2004 [16]. 50 μL 0.155 mM ammonium acetate was added to yeast cell pellets and the suspension was transferred to a glass-coated 96 deep well plate containing 50 μL glass beads per well. Cells were lysed using a Thermomixer C (Eppendorf, 1400 rpm, 2 h, 4 °C). 200 μL of acidified methanol and 500 μL water-washed hexane was added to each sample, and the plate shaken (1000 rpm, 1 min, 4 °C). 300 μL of the hexane layer was removed and 500 μL hexane added, and the plate re-shaken (1000 rpm, 1 min, 4 °C). This was repeated five times with 800 μL hexane removed on the fifth repeat (a total of 2 mL hexane collected). The collected hexane was dried under nitrogen in a fume hood for 1 h at room temperature. The resulting dried lipids were re-dissolved in 150–180 μL ice-cold mobile phase (ethanol:methanol:isopropanol: ammonium acetate pH 4.4, 65:30:3:2, vol/vol/vol/vol) and transferred into HPLC vials. Samples were stored at 4 °C until analysis via HPLC coupled to UV and electrochemical detection (HPLC-UV/ECD) or liquid chromatography tandem mass spectrometry (LC-MS/MS). For HPLC-UV/EC analyses, 100 μL of samples were injected onto a Supelcosil LC-C18 column (5 μm, 250 mm × 4.6 mm) eluted at 1 mL/min and connected to UV and electrochemical (ESA CoulArray 5600A) detectors. Ergosterol was detected at 280 nm, while total CoQ_6 (CoQ_6 + CoQ_6H_2) was detected at −700, +700 and + 700 mV. For studies in which total CoQ_6 (CoQ_6 + CoQ_6H_2) was determined by LC-MS/MS, 2 μL of sample was injected onto an Agilent 1290 UHPLC system connected to an Agilent 6490 triple-quadrupole mass spectrometer. Analytes were separated on a Luna 5 μm C18 (2) 100 Å column (150 × 4.6 mm; Phenomenex, USA) by gradient elution using mobile phase A (2.5 mM ammonium formate in 95:5 methanol:isopropanol) and mobile phase B (2.5 mM ammonium formate in 100% isopropanol) at 0.4 mL/min. The gradient consisted of 50% mobile phase B from 0 to 15 min, 50–70% B from 15 to 17 min, 100% B from 17 to 19 min and back to 50% B from 19 to 24 min. Flow was then directed into the triple quadrupole mass spectrometer with parameters set as follows: gas temperature = 290 °C; gas flow = 14 L/min; nebuliser pressure = 25 psi; sheath gas heater = 400 °C; sheath gas flow = 11 L/min; capillary voltage = 3000 V. Detection of CoQ_6, was by multiple reaction monitoring (MRM) in positive ion mode using the above general mass spectrometry parameters with fragmentor voltage at 380 V and cell accelerator voltage at 5 V. The fragment ion generated by collision-induced dissociation of the $[M + H]^+$ ion was used for quantification. MRM settings for the target analytes were (parent ion → fragment ion); CoQ_6 (*m/z* 591.3.1 → 197.1) with collision energy of 21 V and CoQ_6H_2 (*m/z* 593.3.1 → 197.1) with collision energy of 25 V. CoQ_6, CoQ_6H_2 and ergosterol were quantified against authentic commercial standards obtained from Avanti Polar Lipids and Sigma Aldrich (USA) respectively.

2.3. Determination of S-adenosyl-L-methionine and S-adenosyl-L-homocysteine content in yeast cells and mitochondria

All work was carried out under an argon gas cloud. Yeast pellets were defrosted and 100 μL of 50% methanol containing 100 μM diethylenetriaminepentaacetic acid (DTPA) was added and cell pellets lysed at 40 kpsi (50 s on, 10 s off; 30 cycles at 20 °C) using a Barocycler 2320EXT (Pressure BioSciences Inc). 100 μL chloroform containing 100 μM DTPA was added to the lysate, the suspension mixed vigorously for 1 min, centrifuged (5000×*g*, 5 min, 4 °C), and 50 μL top aqueous layer removed and 100 μL 50% methanol containing 100 μM DTPA added to the sample. The sample was vortexed for 1 min, centrifuged (5000×*g*, 5 min, 4 °C), and 100 μL of the aqueous layer removed (total 150 μL sample collected). Samples were stored at −80 °C until analysis. 5 μL of sample was injected onto an Agilent 1290 UHPLC system connected to an Agilent 6490 triple-quadrupole mass spectrometer. Analytes were separated on a Polar RP 80 Å column 250 × 2.5 mm (Phenomenex, USA) by gradient elution using mobile phase A (0.1% formic acid, 5 μM medronic acid in water) and mobile phase B (0.1% formic acid, 5 μM medronic acid in 100% methanol) at 0.2 mL/min. The gradient consisted of 2% mobile phase B from 0 to 5 min, 2–90% B from 10 to 15 min, 2% B from 15 to 18 min. Flow was then directed into the triple quadrupole mass spectrometer with parameters set as follows: gas temperature = 220 °C; gas flow = 12 L/min; nebuliser pressure = 40 psi; sheath gas heater = 380 °C; sheath gas flow = 12 L/min; capillary voltage = 4000 V. Detection of SAM and SAH was by multiple reaction monitoring (MRM) in positive ion mode using the general mass spectrometry parameters listed above with fragmentor voltage at 380 V and cell accelerator voltage at 4 V. The fragment ion generated by collision-induced dissociation of the $[M + H]^+$ ion was used for quantification. MRM settings for the target analytes were (parent ion → fragment ion); SAM (*m/z* 399.4 → 249.9) with collision energy of 17 and SAH (*m/z* 385.4 → 136.0) with collision energy of 25. SAM and SAH were quantified against commercial standards (Sigma-Aldrich).

For mitochondrial analyses of SAM and SAH, yeast mitochondria were isolated as described [17]. Briefly, cells were grown until; OD_{600} ~1.0 and centrifuged (3000×*g*, 5 min, 4 °C) to pellet cells. Cells were resuspended in 100 mM Tris-H_2SO_4 buffer pH 9.4 containing 10 mM dithiothreitol (DTT) and incubated at 30 °C for 20 min. Cells were centrifuged at 3000×*g* for 5 min at 4 °C and resuspended in Zymolyase buffer (10 mM potassium phosphate pH 7.4, 1.2 M sorbitol). Cells were centrifuged (3000×*g*, 5 min, 4 °C), the supernatant removed, and pellets resuspended in Zymolyase buffer containing Zymolyase 100T and incubated at 30 °C shaking for 1 h. Following washing with Zymolyase buffer, cells were resuspended in homogenization buffer (10 mM Tris-Cl pH 7.4, 0.6 M sorbitol, 1 mM EDTA, 1 mM PMSF, 0.2% (w/v) bovine serum albumin (BSA)) and homogenized with 15 strokes of a Teflon-glass homogenizer. Following removal of cell debris by low-speed centrifugation (1500×*g*, 5 min, 4 °C), the supernatant was centrifuged at 4000×*g* for 5 min at 4 °C and the resulting supernatant centrifuged at 12,000×*g* for 15 min at 4 °C. The resulting mitochondrial pellet was gently resuspended in yeast mitochondrial buffer (1 mM MOPS-KOH pH 7.2, 250 mM sucrose). Protein concentration was determined by BCA assay as per manufacturer's protocol (ThermoFisher Scientific) and samples stored at −20 °C until analysis. On the day of analysis, 50 μg mitochondrial protein was resuspended in 100 μL of 50% methanol containing 100 μM DTPA and extracted as per yeast homogenates, and SAM and SAH concentrations determined by LC-MS/MS as outlined above.

2.4. McArdle-RH7777 hepatoma cell culture

Rat McArdle-RH7777 hepatoma cells stably transfected with a vector containing human PEMT [18] were grown in Dulbecco's Modified Eagle Medium (DMEM, Thermo Fisher Scientific, 11995) containing 10% fetal calf serum (FCS), 4.5 g/L glucose, 110 mg/L sodium pyruvate, 1X GlutaMAX™ (ThermoFisher Scientific) supplemented with penicillin and streptomycin in a humidified atmosphere with 5% CO_2. Cells were incubated with 10 μM 3-deazaadenosine (DZA) or vehicle (water) for 24 h and cells were harvested and stored at −20 °C until mitochondrial CoQ, SAM and SAH were determined as outlined previously.

2.5. 3T3-L1 fibroblast culture and differentiation into adipocytes

Mycoplasma-free 3T3-L1 fibroblasts obtained from Howard Green (Harvard Medical School, Boston, MA) were maintained in Dulbecco's Modified Eagle Medium (DMEM) (Thermo Fisher Scientific, 11995) supplemented with 10% FCS (Thermo Fisher Scientific), 1% GlutaMAX™ (Thermo Fisher Scientific) in a humidified atmosphere with 5% CO_2. Confluent 3T3-L1 cells were differentiated into adipocytes by the addition of DMEM supplemented with 10% FSC and 0.22 μM dexamethasone, 100 ng/mL biotin, 2 μg/mL insulin and 500 μM 3-isobutyl-1-methylxanthine (day zero). After 72 h, medium was replaced with DMEM/10% FCS/GlutaMAX™ containing 2 μg/mL insulin (day three post differentiation) and grown for a further 72 h (day six post differentiation). Cells were used between days 6 and 7 after the initiation of differentiation for all experiments.

2.6. Determination of CoQ content in differentiated 3T3-L1 adipocytes and McArdle RH7777 hepatoma cells

Briefly, cells were homogenized in mitochondrial isolation buffer (10 mM Tris-MOPS, pH 7.4, 1 mM EGTA, 200 mM sucrose containing protease inhibitors) for 30 s at 7000 rpm (Heidolph homogenizer) and samples kept at 4 °C subsequently. 100 μL of the homogenates was kept for total tissue CoQ_9 and CoQ_{10} analyses, and the remaining homogenate was used to isolate mitochondria as previously described [19]. Briefly, homogenates were centrifuged at 700×*g* for 10 min and the supernatant isolated and centrifuged at 7000×*g* for 10 min to obtain a pellet containing the mitochondria. The pellet was re-suspended in mitochondrial isolation buffer and re-centrifuged at 7000×*g* for 10 min. The mitochondrial pellet was finally re-suspended in mitochondrial isolation buffer and protein concentration determined using the BCA assay. CoQ extraction was carried out as previously described [16]. Briefly, 50–100 μL of isolated mitochondria was incubated with 25 μL *para*-benzoquinone (2 mg/mL) for 30 min at room temperature, and 2 mL acidified methanol and 10 mL of water-washed hexane were added. The mixture was mixed vigorously for 1 min, centrifuged (1430×*g*, 5 min, 4 °C) and 9 mL of hexane layer collected and dried using a rotary evaporator. The resulting dried lipids were re-dissolved in 150–180 μL ice-cold mobile phase (ethanol:methanol:isopropanol: ammonium acetate pH 4.4, 65:30:3:2, vol/vol/vol/vol), transferred into HPLC vials and analyzed using HPLC connected to UV and electrochemical detectors as outlined above, or using liquid chromatography tandem mass spectrometry (LC-MS/MS). If LC-MS/MS was used, the dried lipids were resuspended in 150 μL ice-cold HPLC-grade ethanol and analyses carried out as per described previously [11].

2.7. Determination of S-adenosyl-L-methionine and S-adenosyl-L-homocysteine content in liver

Mitochondria from liver tissue was extracted as previously described for mitochondrial CoQ determination. Mitochondrial pellets were resuspended in 100 μL mitochondrial isolation buffer (10 mM Tris-MOPS, pH 7.4, 1 mM EGTA, 200 mM sucrose containing protease inhibitors) and stored at −20 °C until analysis. 50 μL of liver mitochondria were defrosted and 50 μL of 100% methanol containing 100 μM DTPA was added to mitochondria. 100 μL chloroform containing 100 μM DTPA was added to the sample and the suspension mixed vigorously for 1 min, centrifuged (5000×*g*, 5 min, 4 °C). 50 μL of the top aqueous layer was removed and 100 μL 50% methanol containing 100 μM DTPA added to the sample. The sample was vortexed for 1 min, centrifuged (5000×*g*,

5 min, 4 °C), and 100 μL of the aqueous layer removed (total 150 μL sample collected). All sample work up was done under a cloud of argon gas. Samples were stored at −80 °C until analysis. 5 μL of sample was injected onto an TSQ Altis™ Triple Quadrupole Mass Spectrometer (ThermoFisher Scientific). Analytes were separated on a Polar RP 80 Å column 250 × 2.5 mm (Phenomenex, USA) by gradient elution using mobile phase A (0.1% formic acid, 5 μM medronic acid in water) and mobile phase B (0.1% formic acid, 5 μM medronic acid in 100% methanol) at 0.2 mL/min. The gradient consisted of 2% mobile phase B from 0 to 5 min, 2–90% B from 10 to 15 min, 2% B from 15 to 18 min. The triple quadrupole mass spectrometer H-ESI source parameters were set as follows: sheath gas = 58.8 Arb, aux gas = 13.4 Arb, sweep gas = 2.9 Arb, Ion transfer tube temperature = 350 °C, static spray voltage with positive ion voltage set at 4936.36 V and negative ion voltage set at 3500 V. Detection of SAM and SAH, was by multiple reaction monitoring (MRM) in positive ion mode using the above general mass spectrometry parameters. The fragment ion generated by collision-induced dissociation of the $[M + H]^+$ ion was used for quantification. MRM settings for the target analytes were (parent ion → fragment ion); SAM (*m/z* 399.088 → 136.125) with collision energy of 27.03 and RF lens 64 V, SAH (*m/z* 385.088 → 134.042) with collision energy of 19.49 and RF lens 58 V. SAM and SAH were quantified against commercial standards (Sigma-Aldrich). For samples analyzed on the TSQ Altis™ Triple Quadrupole Mass Spectrometer, data was analyzed using Thermo Fisher Scientific™ FreeStyle software.

2.8. Animal studies

All animal procedures were approved by the University of Alberta's Institutional Animal Care Committee (AUP00000175) in accordance with guidelines of the Canadian Council on Animal Care. Mice were exposed to a 12-h light/dark cycle with free access to food and drinking water. Male *Pemt*$^{+/+}$ and *Pemt*$^{-/-}$ (C57BL/6J) mice were fed a standard chow diet (5001; LabDiet, St. Louis, MO, USA) or a semisynthetic high-fat diet (HFD, F3282; Bio-Serv, Flemington, NJ, USA) that contained 60 kcal% from lard. Mice were kept on the appropriate diet for 6–10 weeks and tissue collected and stored at −80 °C until analyses. As previously reported (20), for *in vivo* experiments using control (GFP) adeno-associated virus (AAV.GFP) and PEMT expressing adeno-associated virus (AAV.PEMT) [20], *Pemt*$^{-/-}$ mice were injected with 1×10^{10} genome copies per mouse of AAV.GFP or AAV.PEMT, and *Pemt*$^{+/+}$ mice were injected with an equal dose of AAV.GFP. At 1-week post-AAV administration mice, were fed HFD for 10 weeks [20]. For *in vivo* antisense oligonucleotide (ASO) experiments, male C57BL/6J mice (purchased from Jackson Laboratory, Bar Harbor, ME, USA) were intra-peritoneally injected weekly (25 mg/kg b.w.) with either a scrambled control ASO (5′-GGCCAATACGCCGTCA-3′) or an ASO that inhibits PEMT (5′-CTTTATTAGTGTGTCG-3′), (5′-TTATTAGTGTGTC GGG-3′) or (5′-ACAACATGATTGGACC-3′) provided by Ionis Pharmaceuticals). One week after the first ASO injection, mice were fed the HFD for 10 weeks and tissue collected and stored at −80 °C until analyses. Glucose tolerance tests, insulin tolerance tests and PEMT activity assays in mice treated with ASO were carried out as previously described [20]. For glucose tolerance test data, area under the curve was computed using the trapezoid rule. For insulin tolerance test data, incremental area under the curve was computed. For this, each data point was baseline (0 time) corrected and Δ blood glucose was plotted over time. The area under the Δ blood glucose curve was then calculated using the trapezoid rule.

2.9. Determination of CoQ_9 and CoQ_{10} content in mouse tissue and mitochondria

Tissues were homogenized in mitochondrial isolation buffer (10 mM Tris-MOPS, pH 7.4, 1 mM EGTA, 200 mM sucrose containing protease inhibitors) for 30 s at 7000 rpm (Heidolph homogenizer) and samples kept at 4 °C for all subsequent procedures. 100 μL of the homogenates was kept for total tissue CoQ_9 and CoQ_{10} analyses, and the remaining homogenate was used to isolate mitochondria as previously described [19]. Briefly, homogenates were centrifuged at 700×*g* for 10 min, the supernatant isolated and centrifuged at 7000×*g* for 10 min to obtain a pellet containing mitochondria. The pellet was re-suspended in mitochondrial isolation buffer and re-centrifuged at 7000×*g* for 10 min. The mitochondrial pellet was finally re-suspended in mitochondrial isolation buffer and a BCA assay (Thermo Fischer Scientific) carried out to quantify protein concentration. 50–100 μL of homogenate or isolated mitochondria was placed in a 15 mL screw top tube, 25 μL *para*-benzoquinone (2 mg/ml) was added, incubated for 30 min at room temperature and then 2 mL ethanol: isopropanol (95:5) and 10 mL of water-washed hexane were added. The mixture was mixed vigorously for 1 min, centrifuged (1430×*g*, 5 min, 4 °C) and 9 mL of hexane was collected and dried using a rotary evaporator. The resulting dried lipids were re-dissolved in 150–180 μL ice-cold mobile phase (ethanol:methanol:isopropanol: ammonium acetate pH 4.4, 65:30:3:2, vol/vol/vol/vol) and transferred into HPLC vials. Cholesterol, CoQ_9 and CoQ_{10} were determined by HPLC using a Supelcosil LC-C18 column (5 μm, 250 mm × 4.6 mm) eluted at 1 mL/min connected to UV and electrochemical (ESA CoulArray 5600A) detectors. Non-esterified cholesterol was detected at 214 nm, while CoQ_9 and CoQ_{10} were detected at −700, +700 and + 700 mV and quantified against authentic commercial standards obtained from Sigma Aldrich (USA).

3. Results

3.1. Genome-wide screening identifies 30 novel regulators of CoQ content

To systematically identify the genetic networks controlling CoQ synthesis we conducted a quantitative genome-wide screen of all 5420 mutants contained in the *Saccharomyces cerevisiae* homozygous diploid Deletion Collection [21]. This approach represents an unbiased, global approach to interrogate the CoQ regulatory framework by identifying gene deletions that alter cellular CoQ concentration. To enable large-scale screening by quantitative HPLC coupled to electrochemical detection, we developed an optimized method for cell growth, lysis and CoQ extraction for small culture volumes (~200 μL) in a 96-well plate format (Figs. S1A–C). Intra- and inter-day reproducibility of the method was 3 and 15%, respectively (Fig. S1D), and considered acceptable. The development of this screening method also increased the number of samples processed in one day by about five-fold, from 20 to 96. We then used this method to determine the cellular CoQ concentration in each knockout mutant, with results normalized to cell biomass. The screen was carried out in two phases (Fig. S2A). In both phases cells were grown in minimal media in the absence of any CoQ precursors such as *para*-aminobenzoic acid or 4-hydroxybenzoic acid to reduce confounding results caused by substrate availability. First, all mutants were screened (n = 1), identifying 140 mutants with CoQ content 2 standard deviations higher or lower than the plate population mean. Second, these mutants were re-screened (n = 4–6) against wild-type (WT) cells to confirm gene mutants with significantly altered CoQ content. The genetic screen revealed 30 mutants with significantly higher CoQ ('high CoQ') and seven with significantly lower CoQ ('low CoQ') than WT (Table 1). The 'low CoQ' mutants were comprised entirely of known genes of the biosynthetic pathway, as well as *HFD1* which encodes a dehydrogenase involved in the production of the CoQ precursor, 4-hydroxybenzoic acid [22]. These results validate the approach chosen to identify mutants with altered cellular CoQ content. The 30 'high CoQ' mutants identified were comprised entirely of genes not previously associated with cellular CoQ and represent potential novel CoQ regulators.

We next asked whether the identified 30 'high CoQ' regulators form part of a transcriptional response to altered CoQ by studying the transcriptional profiles of yeast mutants of the CoQ biosynthetic pathway

Table 1
S. cerevisiae mutants identified with significantly decreased or increased CoQ_6 content compared with WT.

'Low CoQ' mutants	
	~Fold decrease in CoQ_6 vs WT
coq2Δ	not detectable
coq3Δ	not detectable
coq4Δ	not detectable
coq6Δ	not detectable
coq8Δ	not detectable
coq9Δ	not detectable
hfd1Δ	2
'High CoQ' mutants	
	~Fold increase in CoQ_6 vs WT
mss116Δ	2
sin3Δ	2
swa2Δ	2
trf5Δ	2
aim26Δ	2
rri1Δ	2
trf4Δ	2
vps54Δ	2
aim9Δ	2
drs2Δ	2.5
atp15Δ	2.5
pac10Δ	2.5
ctk3Δ	2.5
nup60Δ	3
arc1Δ	3
sac1Δ	3
ume6Δ	3
hof1Δ	3
bud31Δ	3
vps20Δ	3
mrpl4Δ	4
pho85Δ	4
rad51Δ	5
srs2Δ	5
cho2Δ	5
rrg7 Δ	7
cdc50Δ	8
ric1Δ	11
ort1 Δ	11
adk1 Δ	12

(*coq1Δ*, *coq3Δ*, *coq7Δ*, *coq8Δ* and *coq9Δ*) grown in the absence and presence of exogenously supplemented CoQ. Gene expression changes in mutants compared to WT (≥2-fold change) were identified. (Supplementary Table 1). Notably, deficiency in any one of the *COQ* genes did not lead to the alteration of the expression of other *COQ* genes for the biosynthesis of CoQ. Of all mutants tested, only deletion of *COQ7* resulted in downregulation of *COQ1* gene expression, with no *COQ* transcripts differentially expressed in any other mutant. There was also no change in the expression of genes identified in our screen, genes previously known to contribute to CoQ synthesis, such as *PTC7* and *HFD1*, or genes involved in isoprenoid or benzoquinone head group synthesis. Comparing gene expression profiles across all *COQ* mutants (Figs. S2B–C), only 5 genes were identified as differentially expressed in the absence of CoQ supplementation (*ARN2*, *FIT2*, *FIT3*, *FDC1* and *YDR514C)* and 7 genes in CoQ supplemented conditions (*ARN1, ARN2*, *FIT2*, *PHO84*, *SIT1*, *TIS11* and *YDR514c*).

Strikingly, the transcriptional changes observed in the various *coq* mutants were not able to be completely reversed by exogenous CoQ supplementation (Supplementary Table 1; Fig. S2C). Thus, exogenous CoQ supplementation may not be able to fully replace endogenous CoQ functions. In addition, CoQ supplementation did not lead to changes in any genes identified in our study, such as *CHO2* or genes identified previously such as *HFD1*. From this it appears that exogenous CoQ supplementation does not, at least transcriptionally, affect endogenous CoQ regulatory pathways.

3.2. A deficiency in phosphatidylethanolamine (PE) methylation results in increased mitochondrial CoQ

Among the top hits was the *cho2Δ* mutant which lacks PEMT, encoded by the *CHO2* gene. The methylation pathway is one of three distinct PC synthesis pathways, along with the Kennedy Pathway and lyso-PC to PC cycling (Fig. 1A). We focused on the *cho2Δ* mutant for the following reasons. First, PEMT activity is evolutionarily conserved in eukaryotes. Second, mice lacking PEMT are viable and have long been known to be protected from atherosclerosis, age-dependent cardiac dysfunction and insulin resistance [23–25], although the underlying reasons for this protective phenotype have remained obscure. Third, PEMT catalyzes the methylation of phosphatidylethanolamine (PE) to phosphatidylcholine (PC), and CoQ biosynthesis requires three methylation steps. Finally, a potential link between PEMT and CoQ has not been investigated to date.

The *cho2Δ* mutant accumulated five times more total CoQ than WT cells (Fig. 1B) and over ten times more mitochondrial CoQ than WT cells (Fig. 1C). Consistent with this, the *cho2Δ* mutant displayed significantly increased concentrations of the CoQ_6 intermediates demethoxy-demethyl-Q_6 ($DDMQ_6$), demethoxy-Q_6 (DMQ_6) and imino-demethoxy-Q_6 ($IDMQ_6$) (Fig. 1D–F). The *cho2Δ*-CoQ relationship was confirmed in multiple yeast strain backgrounds (Figs. S3A and S3B). Mutants heterozygous for *CHO2* did not have altered total or mitochondrial CoQ content (Figs. S3C and S3D). The observed increase in cellular CoQ in *cho2Δ* was reversed by re-expression of *CHO2* (Fig. 1G), indicating that CoQ content is dependent on *CHO2* expression. Isotope tracing studies using $^{13}C_6$-4-hydroxybenzoic acid showed that *cho2Δ* cells have an increased rate of CoQ biosynthesis (Fig. 1H). These results establish that *CHO2* deficiency is a positive regulator of mitochondrial CoQ content.

3.3. PEMT deficiency increases mitochondrial CoQ through a phosphatidylcholine-independent pathway

In yeast, conversion of PE to PC is carried out by two enzymes (Cho2 and Opi3) [26], whereas in mammals PEMT catalyzes all three methylation reactions [27]. Consistent with previous reports, *cho2Δ* mutants had decreased PC (~2-fold) and increased PE concentrations (~1.5-fold) compared to WT cells [28,29] reflecting the role of *CHO2* in PC synthesis (Figs. S3E–G). To test whether altered cellular PC content was responsible for increased CoQ in the *cho2Δ* mutant, *cho2Δ* cells were supplemented with choline to bypass defects in the methylation pathway [28]. This significantly elevated PC concentrations, normalized PE contents (Figs. S3E–F) and restored WT CoQ concentrations (Fig. 1I), consistent with cellular PC or the PC-to-PE ratio regulating CoQ concentrations. Inconsistent with this interpretation, however, supplementation with monomethylethanolamine (MME) also restored WT CoQ content in *cho2Δ* (compare control in Fig. 1I with Fig. S3H) without restoring WT PC-to-PE ratios [28]. Moreover, the *opi3Δ* mutant, which lacks the ability to catalyze the last two methylation steps in PE formation from PC, had significantly lower PC and similar PC-to-PE ratios compared with *cho2Δ* cells (Fig. S3G and S3I-K), yet accumulated ~ four-times less mitochondrial CoQ than *cho2Δ* cells (Fig. S3L). Mutants of the Kennedy pathway also did not have altered CoQ content despite having PC/PE ratios comparable to the *cho2Δ* mutant (Fig. 1J and K). Together, these results indicate that *CHO2*/PEMT modulates cellular CoQ independent of changes in PC and PE content, or changes to the PC-to-PE ratio.

3.4. Mitochondrial CoQ is selectively altered in response to PEMT deficiency

Mitochondrial CoQ synthesis requires three distinct building blocks (Fig. S4A): the 'benzoquinone ring' derived from a tyrosine/ring precursor; the polyisoprenoid 'tail' derived from the mevalonate pathway; and a methyl donor *S*-adenosylmethionine (SAM) required to produce

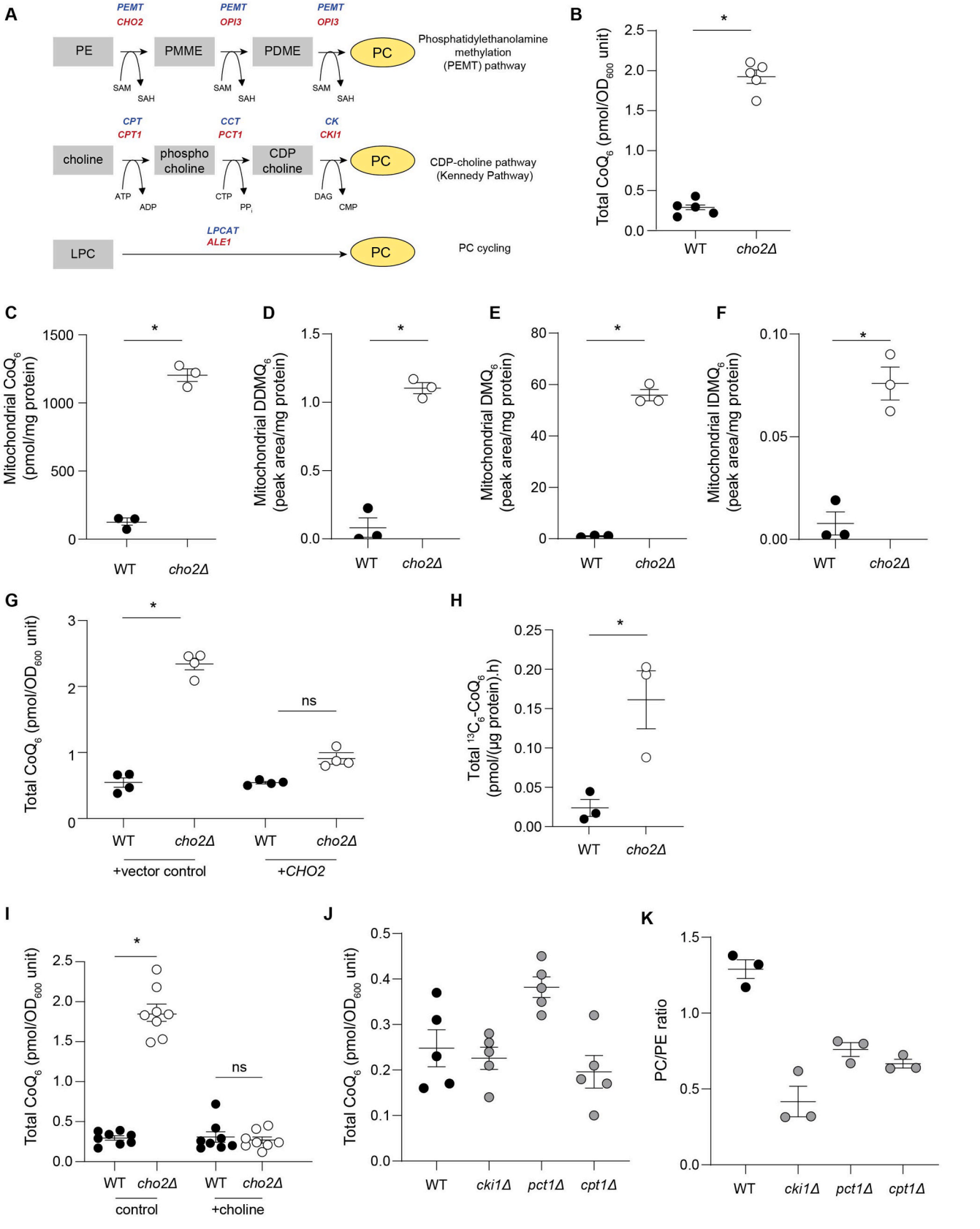

(caption on next page)

Fig. 1. PEMT deficiency is a novel regulator of mitochondrial CoQ_6 content in *S. cerevisiae*. **(A)** Scheme of the three pathways that mediate phosphatidylcholine (PC) synthesis in yeast and mammals; red indicates genes in yeast, while blue indicates mammalian genes. **(B)** Total CoQ_6 concentrations in *cho2Δ* mutants compared with WT (n = 5). **(C)** Mitochondrial CoQ_6 concentrations in *cho2Δ* mutants compared with WT cells (n = 3). **(D)** Mitochondrial demethoxy-demethyl-Q_6 ($DDMQ_6$) concentrations in *cho2Δ* mutants compared with WT cells (n = 3). **(E)** Mitochondrial demethoxy-Q_6 (DMQ_6) concentrations in *cho2Δ* mutants compared with WT cells (n = 3). **(F)** Mitochondrial imino-demethoxy-Q_6 ($IDMQ_6$) concentrations in *cho2Δ* mutants compared with WT cells (n = 3). **(G)** Total CoQ_6 concentrations in WT and *cho2Δ* mutants harboring either control vector or a single copy of *CHO2* (n = 4). **(H)** CoQ_6 biosynthetic rate in *cho2Δ* mutants and WT cells measured using the rate of $^{13}C_6$-CoQ_6 formed from supplemented $^{13}C_6$-4-hydroxybenzoic acid (4HB) (n = 3). **(I)** Total CoQ_6 concentrations in WT and *cho2Δ* mutants with or without 1 mM choline supplementation (n = 8). **(J)** Total CoQ_6 concentrations in WT and mutants of the Kennedy Pathway (n = 5). **(K)** PC/PE ratio in WT and mutants of the Kennedy Pathway (n = 5). Data and error bars depict mean ± s.e.m. *depicts $P \leq 0.05$ and ns indicates 'not significant' as determined by Mann-Whitney (**B**–**F**, **H**) or Kruskal-Wallis (**G**, **I**–**K**) test. (For interpretation of the references to colour in this figure legend, the reader is referred to the Web version of this article.)

the fully substituted benzoquinone ring in CoQ. These building blocks are transported from the cytosol into mitochondria where the synthesis of CoQ takes place. To determine if increased CoQ biosynthesis in *cho2Δ* cells could be explained by a simple increase in mitochondria that provide the 'machinery' for CoQ biosynthesis, mitochondrial mass was assessed by four independent assays: mitochondrial DNA, citrate synthase activity, porin content, and oxygen flux (Figs. S4B–E). All four parameters showed only a modest increase in mitochondrial mass in *cho2Δ,* well below the 10-fold increase in mitochondrial CoQ. We next asked whether mevalonate-derived lipids were altered. Untargeted lipidomics analyses revealed an increase in dolichols in *cho2Δ* (Fig. S4F) in parallel with an increase in expression of genes involved in the dolichol synthesis pathway (Fig. S4G). This suggested flux through the mevalonate pathway may be altered. However, concentrations of ergosterol (the yeast equivalent of mammalian cholesterol) were not altered in *cho2Δ* (Fig. S4H), indicating that it is unlikely an increase in mevalonate pathway flux or farnesyl pyrophosphate availability underpins the alterations in CoQ and dolichols in *cho2Δ*. Supporting this, there was no change in the expression of farnesyl diphosphate synthase (*ERG20)*, or the genes of the mevalonate pathway in *cho2Δ* (Fig. S4I), indicating differential regulation of isoprenoid lipids by *CHO2.* Finally, the increased rate of CoQ biosynthesis was observed in the absence of changes in the transcript or protein levels of presently known members of the CoQ biosynthetic 'machinery' [30] (Figs. S5A–B), although *cho2Δ* displayed a more stabilized CoQ-synthome (Fig. S5C). The stabilization of the CoQ synthome is an intriguing observation and a direct interaction between Cho2p and the CoQ synthome may exist. However, we believe it is more likely that lack of *CHO2* indirectly acts to stabilize the complex by virtue of increasing CoQ content which has been shown to stabilize some Coq polypeptides and potentially stabilize the CoQ synthome [31].

3.5. PEMT deficiency increases CoQ biosynthesis via increasing mitochondrial methylation capacity

To further understand how a deficiency in *cho2* increases mitochondrial CoQ, we performed untargeted metabolomic analyses. This identified numerous metabolites significantly altered in *cho2Δ* compared with WT cells (Fig. 2A and B; Figs. S6A–B), with the greatest differences observed in *S*-adenosylmethionine (SAM) and *S*-adenosylhomocysteine (SAH) (Fig. S6C). Whole-cell SAM was increased while SAH concentrations were decreased in *cho2Δ*, as reported previously [32]. Targeted LC-MS/MS analyses confirmed these results (Fig. 2C and D). Deficiencies in methyltransferases other than *cho2* had no effect on cellular CoQ, SAM and SAH (Figs. S6D–F). Strikingly, mitochondrial SAM and SAH concentrations were both increased in *cho2Δ* (Fig. 2E and F), in sharp contrast to the situation in whole cells. As CoQ biosynthesis requires SAM-dependent methylation of the benzoquinone ring, WT cells were supplemented with the SAM precursor methionine. This caused a ~20-fold increase in cellular and mitochondrial SAM (Figs. S7A–B) yet CoQ was unaffected (Fig. S7C). Methionine supplementation also increased cellular and mitochondrial SAM concentrations in *cho2Δ* mutants, and in this case, CoQ decreased significantly (Fig. S7C). Together, these results show that cellular or mitochondrial SAM concentrations alone do not determine CoQ concentrations.

SAH is a product inhibitor of methyltransferase activity, and the SAM-to-SAH ratio (rather than SAM concentrations alone) is considered to reflect methylation potential. Compared with WT cells, *cho2Δ* mutants had increased cellular and mitochondrial SAM-to-SAH ratios (Fig. 2G) in parallel with increased CoQ. In WT cells, methionine supplementation increased cellular and mitochondrial SAH (Figs. S7D–E) to an extent comparable to that of SAM (Figs. S7A–B), such that there was no change the SAM-to-SAH ratio (Fig. S7F). In *cho2Δ* cells, methionine supplementation had no effect on cellular SAH (Fig. S7D), whereas it significantly increased mitochondrial SAH concentrations (Fig. S7E), such that the mitochondrial SAM-to-SAH ratio decreased (Fig. S7G) in parallel with decreased CoQ. These results suggest that it is the mitochondrial SAM-to-SAH ratio *i.e.*, the methylation capacity of mitochondria that regulates mitochondrial CoQ, although it remains unclear why methionine supplementation differentially affects cellular and mitochondrial SAM and SAH pools.

The methionine cycle, including SAM synthesis, takes place in the cytosol. Cytosolic SAM is then transported into mitochondria by *SAM5* which itself is inhibited competitively by SAH. As *SAM5* expression was not altered in *cho2Δ* mutants (Fig. 2H), we reasoned that their higher mitochondrial SAM-to-SAH ratio reflected a proportionally higher uptake of cytosolic SAM than SAH, thereby increasing the mitochondrial methylation capacity and, as a result, mitochondrial CoQ synthesis. To test this hypothesis, we overexpressed the SAM synthetase *SAM1* in either the cytosol or mitochondria of WT cells. Strikingly, mitochondrial overexpression of *SAM1* increased CoQ almost five-fold, whereas cytosolic overexpression of *SAM1* did not change CoQ (Fig. 2I). These observations, together with the findings that i) increased mitochondrial SAM-to-SAH is a hallmark of *cho2Δ* and ii) decreasing this ratio decreases mitochondrial CoQ, indicate that the mitochondrial SAM-to-SAH ratio is a previously unrecognized key regulator of CoQ biosynthesis and mitochondrial CoQ content.

3.6. PEMT deficiency regulation of mitochondrial CoQ concentrations in evolutionarily conserved

The methylation pathway of PC synthesis is highly conserved in eukaryotes [33] and the impact of PEMT deficiency on phospholipids, triacylglycerols [29] and ceramides [34] (Figs. S8A–B) is mirrored in yeast and mammals. To test if the yeast phenotype was conserved across species, we investigated the effect of PEMT deficiency on mitochondrial CoQ in multiple rodent cell types *in vitro* and *in vivo*. Pharmacological inhibition of PEMT in PEMT-expressing McArdle 7777 rat hepatoma cells (PEMT-McA) with 3-deazaadenosine (DZA) [35] increased mitochondrial CoQ (Fig. 3A). In line with this, livers of $Pemt^{-/-}$ mice fed chow had a significantly increased total (Fig. S8C) and mitochondrial CoQ (Fig. 3B) compared with $Pemt^{+/+}$ littermates. Plasma CoQ, and total and mitochondrial CoQ in skeletal muscle, kidney, brain and white adipose tissue were not changed (Fig. S8D-L), consistent with PEMT expression being limited to the liver in chow-fed animals [36]. Like the situation in yeast, PEMT deficiency did not alter hepatic expression of CoQ biosynthetic pathway genes (Fig. S8M). Consumption of a high fat diet (HFD) doubled total (Fig. S9A) and mitochondrial CoQ (Fig. 3C) in $Pemt^{-/-}$

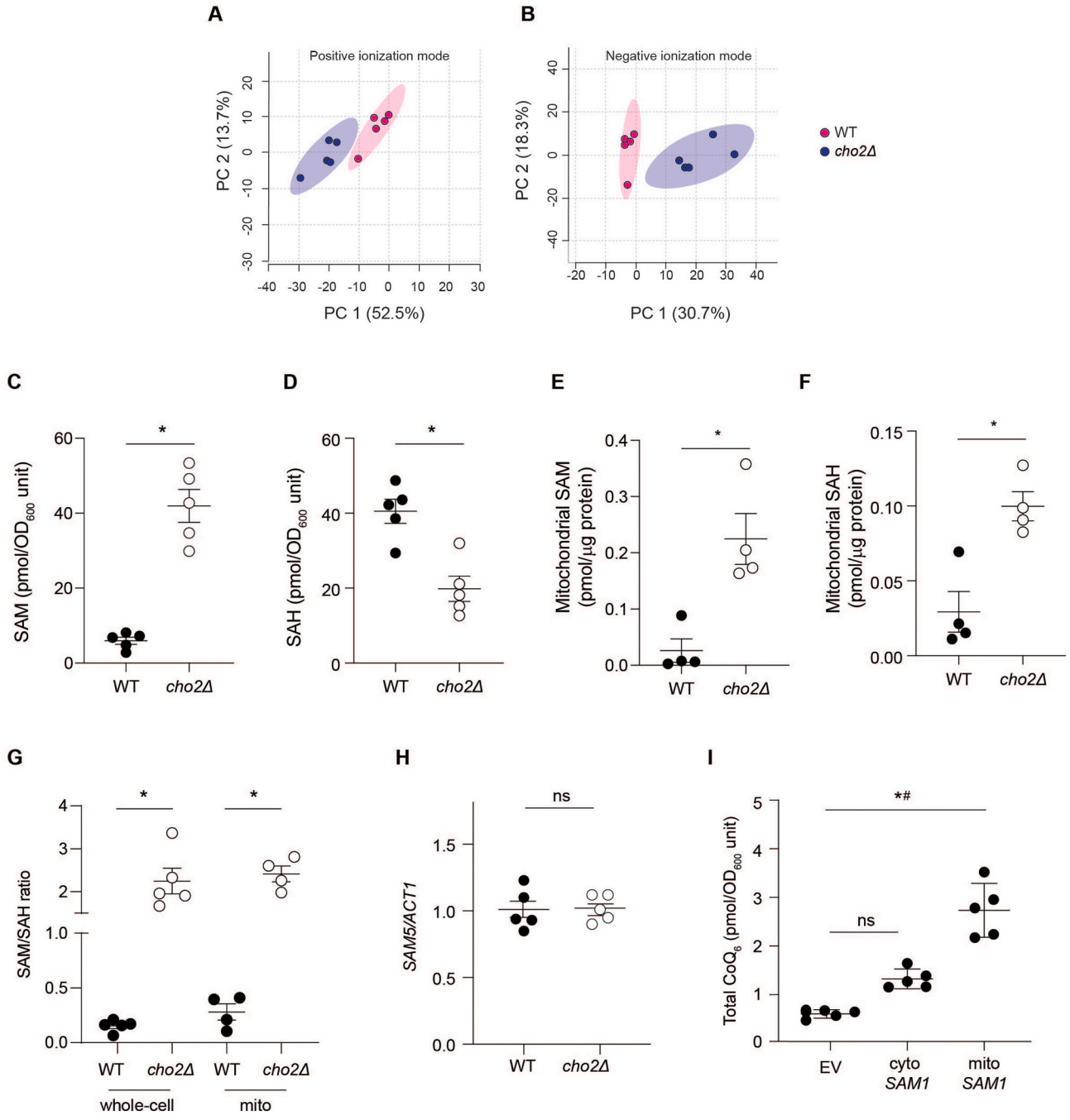

Fig. 2. PEMT deficiency increases CoQ biosynthesis via altering mitochondrial *S*-adenosylmethionine and *S*-adenosylhomocysteine in *S. cerevisiae*. **(A)** Principal component analyses (PCA) plots of metabolites identified in WT and *cho2Δ* in both positive and negative ionization modes. (**B**) Whole cell *S*-adenosylmethionine (SAM) in WT and *cho2Δ* cells (n = 5). (**C**) Whole cell *S*-adenosylhomocysteine (SAH) in WT and *cho2Δ* cells (n = 5). (**E**) Mitochondrial SAM in WT and *cho2Δ* cells (n = 4). (**F**) Mitochondrial SAH in WT and *cho2Δ* cells (n = 4). (**G**) Whole-cell and mitochondrial SAM/SAH ratios in WT and *cho2Δ* cells (n = 4). (**H**) *SAM5* gene expression in WT and *cho2Δ* mutants as measured by qPCR (n = 5). (**I**) The effect of overexpression of *S*-adenosylmethionine synthetase 1 (*SAM1*) either in the mitochondria (mito-*SAM1*) or cytosol (cyto-*SAM1*) compared to empty vector (EV) control on CoQ_6 content in WT. # indicates significant difference between EV and mito-*SAM1*. Data and error bars depict mean ± s.e.m. *$P \leq 0.05$ as determined by Mann-Whitney (**A-H**) or Kruskal-Wallis test (**I**).

mice again without changes in the expression of CoQ biosynthetic pathway genes (Fig. S9B). Normalization of hepatic PEMT activity in $Pemt^{-/-}$ mice using an adeno-associated viral (AAV) system [20] decreased mitochondrial CoQ in the liver to that of $Pemt^{+/+}$ animals expressing control GFP plasmid (Fig. 3D). These results show that PEMT expression regulates mitochondrial CoQ content in hepatic cell lines and the liver of mice, without apparent changes in the canonical CoQ biosynthetic pathway.

We next investigated a potential role of PEMT in the regulation of CoQ concentration in non-hepatic cells. *PEMT* expression was induced during adipocyte differentiation (Fig. S9C), consistent with previous studies [37]. Inhibition of *Pemt* expression in 3T3-L1 adipocytes using anti-sense oligonucleotides (ASO; Fig. 3E) significantly increased mitochondrial CoQ (Fig. 3F). Moreover, we observed a significant increase in total (Fig. S9D) and mitochondrial CoQ (Fig. 3G) in white adipose tissue of $Pemt^{-/-}$ mice fed a high fat diet, conditions where PEMT expression is induced in adipose tissue [37]. Together, these results show that *PEMT* expression can regulate mitochondrial CoQ content in hepatocytes and adipocytes *in vitro* and *in vivo*, as observed in yeast.

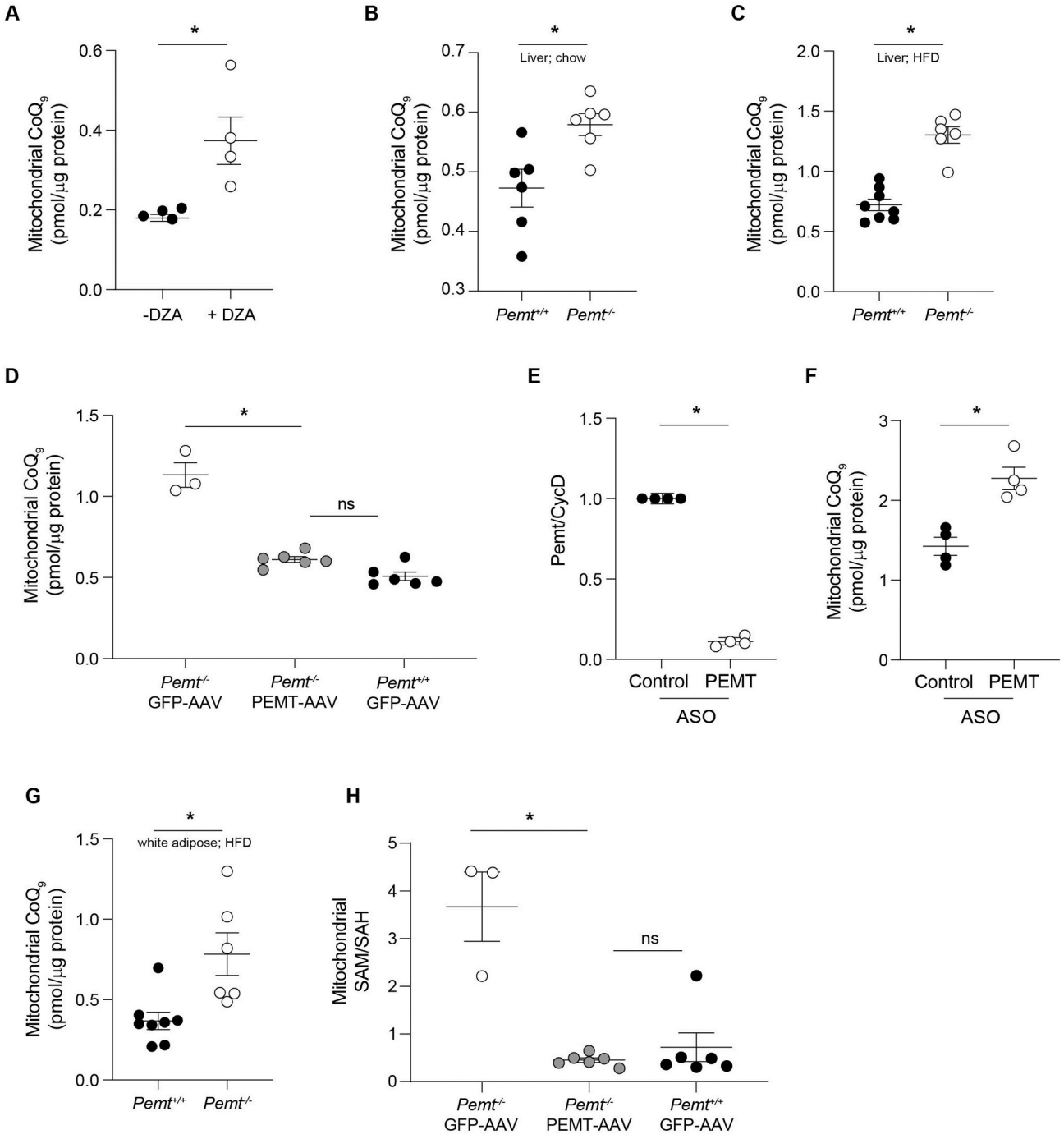

Fig. 3. PEMT deficiency increases mitochondrial CoQ content in mammalian cells and tissues. (**A**) Effect of inhibiting PEMT activity in PEMT-expressing McArdle 7777 hepatoma cells by 3-deazaadenosine (DZA) on mitochondrial CoQ_9 content (n = 4). (**B**) Hepatic mitochondrial CoQ_9 content in $Pemt^{+/+}$ and $Pemt^{-/-}$ mice fed chow (n = 6). (**C**) Hepatic mitochondrial CoQ_9 content in $Pemt^{+/+}$ and $Pemt^{-/-}$ mice fed HFD for 6 weeks (n = 6–8). (**D**) Mitochondrial CoQ_9 content in mice treated with adeno-associated virus (AAV) expressing *Pemt* or GFP control (n = 3–6). (**E**) Effect of anti-sense oligonucleotide (ASO) mediated knockdown of PEMT in differentiated 3T3-L1 adipocytes on PEMT gene expression as determined by qPCR (n = 4). (**F**) Mitochondrial CoQ_9 content in differentiated 3T3-L1 adipocytes treated with either control or anti-PEMT ASO (n = 4). (**G**) White adipose tissue mitochondrial CoQ_9 content in $Pemt^{+/+}$ and $Pemt^{-/-}$ mice fed HFD for 6 weeks (n = 6–8) (**H**) Mitochondrial SAM/SAH ratio in mice treated with adeno-associated virus (AAV) expressing *Pemt* or GFP control (n = 3–6). Data and error bars depict mean ± s.e.m. $^*P \leq 0.05$ and ns indicates 'not significant' as determined by Mann-Whitney (**A-C, E-G**) or Kruskal-Wallis test (**D, H**).

3.7. Mitochondrial SAM-to-SAH ratio is a central feature of PEMT deficiency

A previous commentary [38] suggested that hepatic PEMT was a major component of whole body SAM utilization. A separate investigation reported no difference in hepatic SAM and SAH concentrations in $Pemt^{-/-}$ compared with $Pemt^{+/+}$ mice [39] although mitochondrial SAM and SAH concentrations were not independently measured. We therefore examined whether PEMT expression regulated mitochondrial CoQ in liver through specific changes in the mitochondrial SAM-to-SAH ratio using the previously described AAV system. Compared with WT animals, livers from $Pemt^{-/-}$ mice expressing GFP (control) had significantly increased mitochondrial SAM-to-SAH ratio (Fig. 3H), paralleling their increase in mitochondrial CoQ (Fig. 3D). Expression of *Pemt* in $Pemt^{-/-}$

mice decreased the mitochondrial SAM-to-SAH ratio to levels observed in *Pemt*$^{+/+}$ mice, again in parallel with the observed normalization of mitochondrial CoQ (Fig. 3D). Thus, PEMT expression affects the SAM-to-SAH ratio in mitochondria. Together the data indicate that lowering PEMT expression is sufficient to increase both the mitochondrial SAM-to-SAH ratio and mitochondrial CoQ content, and this relationship is maintained in a broad range of species.

3.8. PEMT deficiency protects against insulin resistance via modulating CoQ and decreasing mitochondrial oxidative stress

We next examined whether regulating mitochondrial CoQ via PEMT can be exploited to ameliorate disease associated with CoQ deficiency. To do this, we focused on insulin resistance for three reasons. First, *Pemt*$^{-/-}$ mice are protected from insulin resistance [25,40] via a currently unexplained mechanism. Second, decreased mitochondrial CoQ is an up-stream driver of insulin resistance in humans, mice, and cellular models [11,41,42], and CoQ supplementation reverses insulin resistance. Third, increasing mitochondrial CoQ decreases mitochondrial superoxide [11] another upstream driver of insulin resistance. We therefore first examined the effect of PEMT deficiency on mitochondrial superoxide. Compared with WT cells, *cho2Δ* mutants had decreased mitochondrial superoxide, as assessed by MitoSOX fluorescence (Fig. S9E). Similarly, *cho2Δ* cells were also protected from decreased viability induced by polyunsaturated fatty acids (Fig. S9F), consistent with superoxide being the primordial reactive oxygen species that can give rise to cell damage via oxidation of unsaturated fatty acids. These results indicate that PEMT deficiency decreases mitochondrial oxidative stress.

To more directly link mitochondrial CoQ and PEMT, we used antisense oligonucleotide (ASO) technology in differentiated 3T3-L1 adipocytes treated with tumour necrosis factor-α (TNFα) as a cellular model of insulin resistance [43]. Decreasing PEMT expression by ASO treatment increased mitochondrial CoQ concentrations above that seen in control ASO-treated cells (Fig. 4A) without a change in insulin-stimulated 2-deoxyglucose uptake (Fig. 4B). Exposure of control ASO-treated adipocytes to TNFα decreased mitochondrial CoQ (Fig. 4A) and insulin-stimulated 2-deoxyglucose uptake (Fig. 4B). Similarly, pharmacological blockade of CoQ synthesis with 4-nitrobenzoic acid (4NB, a competitive inhibitor of 4-hydroxybenzoate:polyprenyltransferase) [44], decreased mitochondrial CoQ (Fig. 4A) in control ASO-treated cells to a comparable extent to that seen with TNFα treatment. This was associated with a comparable decrease in insulin-stimulated glucose uptake (Fig. 4B), consistent with a causal link between mitochondrial CoQ and insulin sensitivity [11]. Replacing control with anti-Pemt ASO restored mitochondrial CoQ and insulin-stimulated 2-deoxyglucose uptake to control values in both TNFα- and 4NB-treated cells (Fig. 4A and B). The results suggest that enhanced CoQ biosynthesis is required for PEMT deficiency to improve glucose utilization in a cellular model of insulin resistance.

Finally, we examined how improved insulin sensitivity *in vivo* via decrease in PEMT activity relates to the mitochondrial SAM-to-SAH ratio. Anti-Pemt ASO significantly decreased hepatic PEMT activity in mice fed HFD (Fig. 4C) and such mice had improved glucose clearance (Fig. 4D) and insulin sensitivity (Fig. 4E). This was evidenced by a decreased area under the curve (AUC) for the glucose tolerance test (GTT), and an increased incremental area under the curve (iAUC) for insulin tolerance test (ITT) (see Fig. S9G for baseline corrected ITT values). Improved glucose clearance and insulin sensitivity were associated with an increase in mitochondrial CoQ, SAM and SAM-to-SAH ratio (Fig. 4F–H), recapitulating the situation in global *Pemt*$^{-/-}$ mice. Together, these data provide a mechanism for how PEMT deficiency ameliorates insulin resistance, *i.e.*, by increasing mitochondrial SAM-to-SAH ratio and CoQ synthesis, a known driver of insulin resistance (Fig. 4I).

4. Discussion

This study outlines the discovery of PEMT deficiency as the first identified positive regulator of mitochondrial CoQ content in organisms from budding yeast to mammals. PEMT regulates CoQ concentrations via modulation of the mitochondrial SAM-to-SAH ratio that determines the methylation reactions required for CoQ biosynthesis. Changes in CoQ are not dependent on altering cellular SAM concentrations or the SAM-to-SAH ratio *per se*, but rather a case of modulating the balance of mitochondrial metabolites, *i.e.*, the 'right ratio in the right place'. This interplay between SAM and PEMT is independent of the cellular PE-to-PC ratio, and it establishes a previously unrecognized functional relationship between PEMT, mitochondrial one-carbon metabolism and CoQ synthesis. Our discovery has potential medical implication because increasing mitochondrial CoQ via PEMT knockdown decreases mitochondrial oxidative stress and it maintains insulin sensitivity *in vivo*. At a mechanistic level, the biological benefit of PEMT knockdown is affected by increasing mitochondrial CoQ and a resulting decrease in superoxide, two known key drivers of insulin resistance. Together, this work enhances our understanding of how cells regulate mitochondrial CoQ synthesis and how this may be translated to a conceptually novel approach to treat insulin resistance.

Our key finding of PEMT as a conserved regulator of mitochondrial CoQ content is supported by work in budding yeast, mammalian cell culture models and *in vivo* mouse studies. Combining the classical genetic approach of gene knockout and re-expression with targeted LC-MS/MS analysis, a direct relationship between PEMT expression and mitochondrial CoQ content was established. Significantly, re-introduction of PEMT expression normalized mitochondrial CoQ concentrations in both budding yeast and mouse models. Acute PEMT disruption mediated by small molecules such as 3-deazaadenosine or antisense oligonucleotides was also sufficient to increase mitochondrial CoQ, recapitulating the results from the genetic approach. Collectively these data confirm that modulation of PEMT at the gene, mRNA or enzyme activity level increases mitochondrial CoQ in a variety of species.

Our studies establish that spatial compartmentalization of the one-carbon metabolites SAM and SAH in mitochondria is necessary for changes in CoQ concentrations and the underlying basis of the PEMT-CoQ relationship. Use of untargeted 'global' metabolomics and targeted sub-compartmental measurements led to the identification of increased SAM-to-SAH ratio in mitochondria across models of PEMT deficiency, paralleling the changes observed in mitochondrial CoQ. Changes (up or down) to the mitochondrial SAM-to-SAH ratio were sufficient to alter mitochondrial CoQ. Mitochondrial CoQ concentrations were unaffected by cytosolic expression of SAM synthetase (*SAM1*) whereas ectopic expression of *SAM1* in mitochondria increased mitochondrial CoQ. These results demonstrate that it is mitochondrial rather than 'cellular' SAM and SAH *per se*, that are the key in modulating mitochondrial CoQ content, and more generally highlight the importance of measuring metabolites at subcellular resolution.

Several lines of evidence support the conclusion that increasing mitochondrial CoQ via attenuated PEMT and the enhanced mitochondrial SAM-to-SAH ratio is beneficial in the context of insulin resistance. We found increasing mitochondrial CoQ via ASO-mediated PEMT knockdown resulted in maintenance of glucose uptake in adipocytes in the presence of TNFα. Increasing mitochondrial CoQ via ASO-mediated PEMT knockdown also maintained glucose uptake in the presence of 4-nitrobenzoic acid. 4-Nitrobenzoic acid is an inhibitor of COQ2, but its inhibitory action on CoQ synthesis and hence CoQ content was ameliorated by the ASO-mediated PEMT knock down. These results suggest that improved glucose uptake in PEMT-deficient cells is causally related to increased (or preserved) CoQ content. Importantly, this causal relationship extends to the *in vivo* situation: modulation of PEMT activity by ASO in HFD-fed mice led to maintenance of insulin sensitivity with improved glucose and insulin responses, and this was associated with a

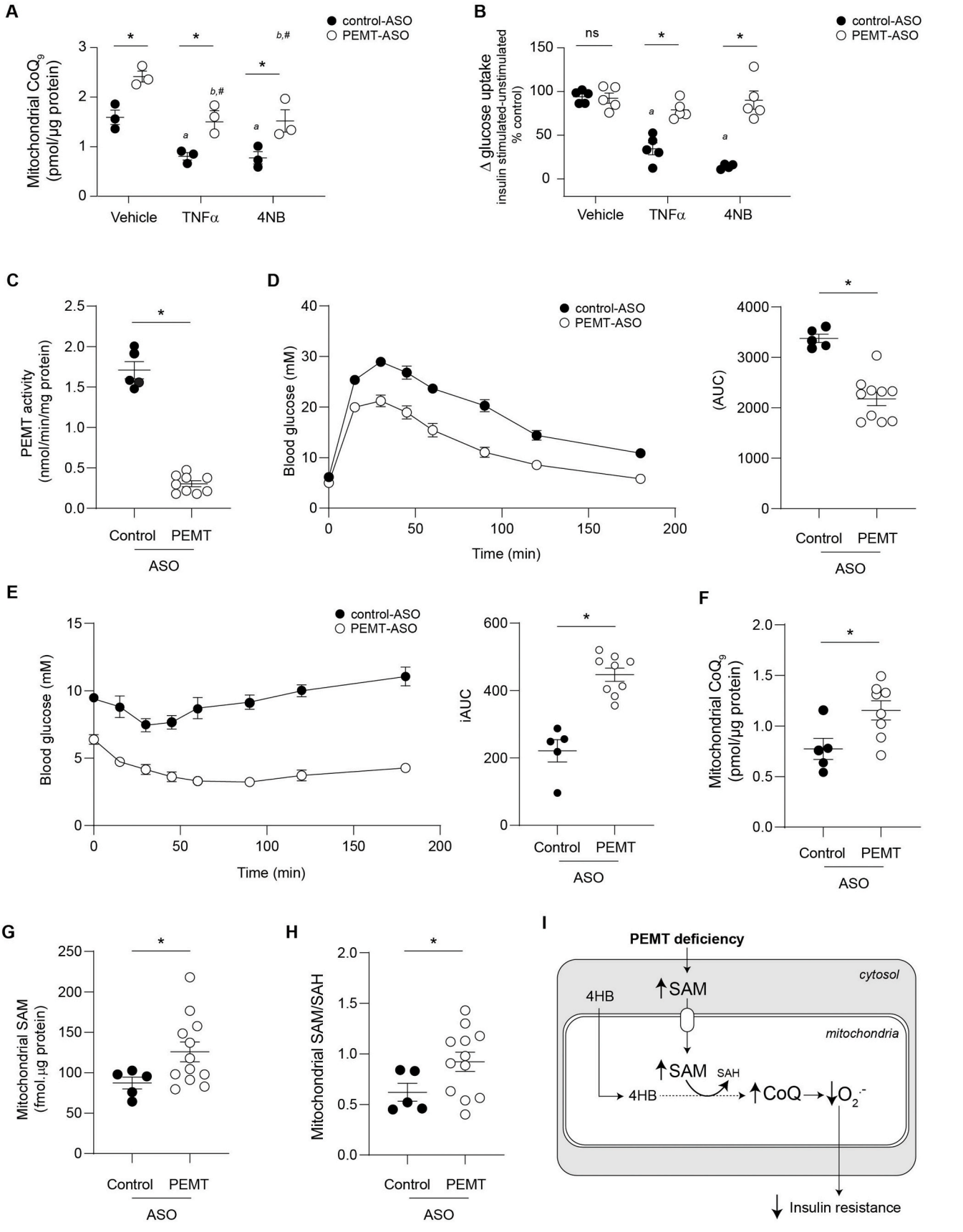

(caption on next page)

Fig. 4. Protection against IR by PEMT deficiency depends on increased mitochondrial CoQ content. (**A**) Mitochondrial CoQ_9 content in 3T3-L1 adipocytes treated with control or anti-Pemt ASO, and TNFα (chronic low dose inflammation inducer) or 4-nitrobenzoic acid (4NB, an inhibitor of CoQ biosynthesis) (n = 3). *Significant difference between control and PEMT-ASO in the same treatment group. [a]Significant difference between TNFα and 4NB treatments compared with vehicle in control-ASO treated cells. [b]Significant difference between TNFα and 4NB treatments compared with vehicle in PEMT-ASO treated cells. [#]No significant difference between cells treated with PEMT-ASO and TNFα or 4NB compared with vehicle-treated control-ASO cells. (**B**) Glucose uptake in 3T3-L1 adipocytes treated with control or anti-Pemt ASO, and TNFα (chronic low dose inflammation inducer) or 4-nitrobenzoic acid (4NB, an inhibitor of CoQ biosynthesis) as measured by uptake of ^{3}H-2-deoxyglucose (n = 5). *ns denotes significant difference or lack thereof, respectively, between control and PEMT-ASO in the same treatment group. [a]Significant difference between TNFα and TNFα+4NB treatments compared with vehicle in control-ASO treated cells. [#]No significant difference between cells treated with PEMT-ASO and TNFα or 4NB compared with vehicle-treated control-ASO cells. (**C**) PEMT activity in C57BL/6J mice fed HFD treated with either control or anti-PEMT ASO for 10 weeks (n = 5–9). (**D**) Glucose tolerance test (GTT) in C57BL/6J mice fed HFD treated with either control or anti-PEMT ASO for 10 weeks (n = 5–10). For area under the curve (AUC), each data point represents the area under the curve extrapolated per animal from blood glucose concentrations determined over 3 h post glucose challenge. AUC was determined as outlined in the Methods. (**E**) Insulin tolerance test (ITT) in C57BL/6J mice fed HFD treated with either control or anti-PEMT ASO for 10 weeks (n = 5–10). For incremental area under the curve (iAUC), blood glucose concentrations per animal were baseline (0 min) corrected, and iAUC calculated from Δ blood glucose concentrations determined over 3 h post insulin challenge. (**F**) Mitochondrial CoQ_9 concentrations in C57BL/6J mice fed HFD treated with either control or anti-PEMT ASO for 10 weeks (n = 5–12). (**G**) Mitochondrial SAM concentrations in C57BL/6J mice fed HFD treated with either control or anti-PEMT ASO for 10 weeks (n = 5–12). (**H**), Mitochondrial SAM/SAH ratio in C57BL/6J mice fed HFD treated with either control or anti-PEMT ASO for 10 weeks (n = 5–12). **(I)** Schematic summary of results and proposed mechanism. PEMT deficiency increases cytosolic SAM resulting in increased mitochondrial SAM and SAM/SAH. Increased mitochondrial SAM increases CoQ biosynthesis by donating methyl groups to the benzoquinone head group of CoQ formed from 4-hydroxybenzoic acid (4HB). Increased mitochondrial CoQ results in decreased mitochondrial superoxide, an upstream driver of insulin resistance. Data and error bars depict mean ± s.e.m. *$P \leq 0.05$ as determined by Mann-Whitney (**C–H**) or Kruskal-Wallis test (**A, B**).

parallel increase in mitochondrial SAM-to-SAH ratio and CoQ in the livers of these mice. As mitochondrial superoxide is a known driver of insulin resistance downstream of CoQ [11,42] and is decreased in PEMT deficiency, our results also uncover a previously unrecognized causal relationship between PEMT and mitochondrial oxidant(s).

In addition to PEMT, our initial screen in conjunction with the yeast knockout collection, identified 30 previously unrecognized regulators of CoQ content in yeast. The genes identified in our study add to the set of gene mutants identified previously [45] as altering total CoQ content. There is limited overlap between the groups of gene mutants identified in each study. This is likely explained by the different growth conditions used, with cellular CoQ content known to be affected by the abundance of benzoquinone head group precursors and cellular metabolic activity. This highlights the complexity of the metabolic factors that govern CoQ synthesis and the need to consider the interaction of metabolic and genetic regulators. Similarly in our study, mutants were selected for further analyses based on their relative CoQ content compared to other mutants grown on the same 96-well plate as meaningful intra-plate comparisons were not feasible. We cannot exclude the possibility that some mutants were missed in our screen, especially those that display a change in CoQ lower than the threshold of the screen.

While we developed the quantitative screening method for yeast cells, it could be applied to most biological samples and hence aid large-scale studies, *e.g.*, clinical studies requiring CoQ measurement. Most of the yeast genes identified have a functional mammalian homolog, raising the possibility for these genes to be additional conserved regulators of cellular CoQ content in mammalian cells. Gene ontology (GO) analyses via FunSpec [46] identified 35 GO Biological Processes as enriched in the 'high CoQ' mutants, none of which have previously been associated with CoQ synthesis. The biological processes identified in the 'high CoQ' mutant groups are in various cellular compartments in addition to mitochondria, *e.g.*, endoplasmic reticulum, the Golgi network, and the nucleus. This suggests that several extra-mitochondrial processes regulate cellular CoQ content, further emphasizing the complex interplay between spatially distinct pathways in the regulation of cellular CoQ concentrations, as we have demonstrated in the case of PEMT deficiency. The development of techniques such as MALDI-imaging to analyze CoQ distribution *in vivo* [47] could aid in the study of such issues, especially in more complex tissues.

Our study raises several interesting questions, *e.g.*, how mitochondrial concentrations of SAM and SAH are regulated, and the potential of our findings for translation to treat CoQ deficiency and related pathologies. What is clear from our studies is that changes in cytosolic SAM concentrations alone are not sufficient to increase mitochondrial SAM or the mitochondrial SAM-to-SAH ratio, and that the mitochondrial SAM-to-SAH ratio does not always reflect the whole-cell situation. While PEMT deficiency increases mitochondrial SAM-to-SAH ratio to beneficially affect mitochondrial CoQ and cell function, ablation of PEMT as a therapeutic strategy poses significant challenges due to the impact of PEMT deficiency on hepatic lipid metabolism. *Pemt*$^{-/-}$ mice fed regular chow diet display no phospholipid defects [36], most likely due to the increased activity of the rate limiting step in the Kennedy Pathway. However, *Pemt*$^{-/-}$ mice fed a high-fat diet display decreased PC (~25%) and a decreased PC/PE ratio [25]. These mice eventually develop severe triglyceride accumulation, endoplasmic reticulum stress and non-alcoholic steatohepatitis (NASH) most likely due to a loss of membrane integrity induced by the decreased PC/PE ratio [48]. Polymorphisms in the *PEMT* gene area associated with non-alcoholic fatty liver disease in humans [49]. Nevertheless, understanding how PEMT deficiency leads to increased mitochondrial SAM-to-SAH ratio may ultimately lead to novel strategies to increase CoQ concentrations *in vivo*.

The methionine cycle is a centre piece of the methylation pathway and occurs in the cytosol. SAM must be transported into mitochondria and the SAH generated must be transported back to the cytosol for either conversion back to SAM or for cysteine/glutathione synthesis. It is likely that other factors affect how much SAM is transported into the mitochondria in PEMT deficiency. One potential factor could be the sub-cellular localization of PEMT. PEMT is localized to ER-mitochondria associated membranes (MAMs) [50], an interface for crosstalk between the ER and mitochondria that is integral in the appropriate functioning of both organelles. Therefore, it seems plausible that PEMT deficiency increases SAM locally in ER-MAM microdomains and that this facilitates SAM accessibility to CoQ biosynthetic complex and mitochondrial CoQ synthesis. In support this, FKBP8 is a regulator of the formation of the ER-mitochondria interface [51] that interacts with COQ9 [52], a protein essential for the stabilization of the putative CoQ biosynthetic complex [53]. COQ polypeptides that participate in the CoQ synthome are also highly enriched at ER-MAM sites [54,55]. These enzymes include COQ3, a SAM-dependent methyltransferase responsible for both *O*-methylation steps in CoQ biosynthesis. We speculate that the increased SAM-SAH-ratio observed in mitochondria of PEMT-deficient cells is driven by the spatial co-enrichment of PEMT and CoQ biosynthetic enzymes in ER-MAM microdomains. If so, this may be an example of redox control at the ER-mitochondrial interface, a sub-cellular location also important in glucose metabolism and insulin signaling [56].

Undoubtedly further studies are necessary to fully understand the complex issues raised by the present study and to harness its potential to develop novel strategies to increase mitochondrial CoQ and overcome mitochondrial oxidative stress and dysfunction resulting from CoQ deficiency. Nevertheless, our work identifies a new network of genes that regulate CoQ, opening the door for further research in this area. In

addition, the identification of the intersection of phospholipid metabolism, mitochondrial one-carbon metabolism, and CoQ synthesis in PEMT deficiency, and how these interact in the setting of insulin resistance represents an exciting advance in our understanding of one-carbon metabolism, lipid biology and mitochondrial function.

Author contributions

AA and RS conceived the work; AA, DJF, SGC, IWD, JWKH, DEV, CFC, RLJ and RS designed the experiments; AA, DJF, GJM, CS, DS, KJL, MCB, LFdR, AY, JWKH, ST, SMYK, and JNV acquired or analyzed data; AA, DJF, SGC, IWD, DEV, CFC, RLJ and RS interpreted data; AA and RS drafted the work or substantially revised the text.

Declaration of competing interest

The authors declare no competing interests.

Acknowledgments

We thank Dr Gustav Dallner (Karolinska Institutet, Stockholm Sweden) for helpful advice. We also thank Ionis Pharmaceuticals (Carlsbad, CA, USA) for providing ASOs. This research was supported by grants from the Australian Research Council (DP150102408 to RS, CFC, IWD), the National Health and Medical Research Council of Australia (NHMRC1052616 to RS) and the Canadian Institutes of Health Research (MOP 5182 to DEV, RLJ, JnV; and MOP 33505 to RLJ). RS was supported by NH&MRC Senior Principal Research Fellowship (1111632), AY was supported by an Australian Post-graduate Award, and SGC was supported by a grant from the National Science Foundation (MCB-1714569). We thank New South Wales Government Office for Health and Medical Research for infrastructure support. We also thank David Fuentes and Atul Bhatnagar of Sydney Mass Spectrometry for assistance and advice with the mass spectrometry analysis carried out at Sydney Mass Spectrometry, a core research facility at the University of Sydney.

Appendix A. Supplementary data

Supplementary data to this article can be found online at https://doi.org/10.1016/j.redox.2021.102127.

References

[1] K. Bersuker, et al., The CoQ oxidoreductase FSP1 acts parallel to GPX4 to inhibit ferroptosis, Nature 575 (2019) 688–692.
[2] C. Mao, et al., DHODH-mediated ferroptosis defence is a targetable vulnerability in cancer, Nature 593 (2021) 586–590.
[3] H. Hoogland, et al., A steady-state study on the formation of Compounds II and III of myeloperoxidase, Biochim. Biophys. Acta 955 (1988) 337–345.
[4] C.M. Anderson, et al., Dependence of brown adipose tissue function on CD36-mediated coenzyme Q uptake, Cell Rep. 10 (2015) 505–515.
[5] M. Alcázar-Fabra, F. Rodríguez-Sánchez, E. Trevisson, G. Brea-Calvo, Primary coenzyme Q deficiencies: a literature review and online platform of clinical features to uncover genotype-phenotype correlations, Free Radic. Biol. Med. 167 (2021) 141–180.
[6] K. Folkers, S. Vadhanavikit, S.A. Mortensen, Biochemical rationale and myocardial tissue data on the effective therapy of cardiomyopathy with coenzyme Q10, Proc. Natl. Acad. Sci. U.S.A. 82 (1985) 901–904.
[7] S.R. Thomas, P.K. Witting, Stocker, A role for reduced coenzyme Q in atherosclerosis? Biofactors 9 (1999) 207–224.
[8] J.M. Letters, et al., Time-dependent changes to lipids and antioxidants in plasma and aortas of apolipoprotein E knockout mice, J. Lipid Res. 40 (1999) 1104–1112.
[9] P.K. Witting, K. Pettersson, J. Letters, R. Stocker, Anti-atherogenic effect of coenzyme Q_{10} in apolipoprotein E gene knockout mice, Free Radic. Biol. Med. 29 (2000) 295–305.
[10] S.L. Molyneux, et al., Coenzyme Q10: an independent predictor of mortality in chronic heart failure, J. Am. Coll. Cardiol. 52 (2008) 1435–1441.
[11] D.J. Fazakerley, et al., Mitochondrial CoQ deficiency is a common driver of mitochondrial oxidants and insulin resistance, Elife 7 (2018), e32111.
[12] A. Ayer, P. Macdonald, R. Stocker, CoQ_{10} function and role in heart failure and ischemic heart disease, Annu. Rev. Nutr. 35 (2015) 175–213.
[13] A.M. Awad, et al., Chromatin-remodeling SWI/SNF complex regulates coenzyme Q (6) synthesis and a metabolic shift to respiration in yeast, J. Biol. Chem. 292 (2017) 14851–14866.
[14] A. Martin-Montalvo, et al., The phosphatase Ptc7 induces coenzyme Q biosynthesis by activating the hydroxylase Coq7 in yeast, J. Biol. Chem. 288 (2013) 28126–28137.
[15] M.T. Veling, et al., Multi-omic mitoprotease profiling defines a role for Oct1p in coenzyme Q production, Mol. Cell. 68 (2017) 970–977 e911.
[16] C.A. Gay, R. Stocker, Simultaneous determination of coenzyme Q10, cholesterol, and major cholesterylesters in human blood plasma, Methods Enzymol. 378 (2004) 162–169.
[17] C. Meisinger, N. Pfanner, K.N. Truscott, Isolation of yeast mitochondria, Methods Mol. Biol. 313 (2006) 33–39.
[18] A.A. Noga, Y. Zhao, D.E. Vance, An unexpected requirement for phosphatidylethanolamine *N*-methyltransferase in the secretion of very low density lipoproteins, J. Biol. Chem. 277 (2002) 42358–42365.
[19] J.M. Daniel, S.D. Friess, S. Rajagopalan, S. Wedt, R. Zenobi, Quantitative determination of noncovalent binding interactions using soft ionization mass spectrometry, Int. J. Mass Spectrom. 216 (2002) 1–27.
[20] S. Wan, et al., Hepatic PEMT activity mediates liver health, weight gain, and insulin resistance, FASEB. J. 33 (2019) 10986–10995.
[21] E.A. Winzeler, et al., Functional characterization of the *S. cerevisiae* genome by gene deletion and parallel analysis, Science 285 (1999) 901–906.
[22] L.A. Payet, et al., Mechanistic details of early steps in coenzyme Q biosynthesis pathway in yeast, Cell. Chem. Biol. 23 (2016) 1241–1250.
[23] Y. Zhao, et al., Lack of phosphatidylethanolamine *N*-methyltransferase alters plasma VLDL phospholipids and attenuates atherosclerosis in mice, Arterioscler. Thromb. Vasc. Biol. 29 (2009) 1349–1355.
[24] L.K. Cole, V.W. Dolinsky, J.R. Dyck, D.E. Vance, Impaired phosphatidylcholine biosynthesis reduces atherosclerosis and prevents lipotoxic cardiac dysfunction in $ApoE^{-/-}$ mice, Circ. Res. 108 (2011) 686–694.
[25] R.L. Jacobs, et al., Impaired de novo choline synthesis explains why phosphatidylethanolamine *N*-methyltransferase-deficient mice are protected from diet-induced obesity, J. Biol. Chem. 285 (2010) 22403–22413.
[26] M.I. Kanipes, S.A. Henry, The phospholipid methyltransferases in yeast, Biochim. Biophys. Acta 1348 (1997) 134–141.
[27] D.E. Vance, Phospholipid methylation in mammals: from biochemistry to physiological function, Biochim. Biophys. Acta 1838 (2014) 1477–1487.
[28] E.F. Summers, V.A. Letts, P. McGraw, S.A. Henry, *Saccharomyces cerevisiae cho2* mutants are deficient in phospholipid methylation and cross-pathway regulation of inositol synthesis, Genetics 120 (1988) 909–922.
[29] G. Thibault, et al., The membrane stress response buffers lethal effects of lipid disequilibrium by reprogramming the protein homeostasis network, Mol. Cell. 48 (2012) 16–27.
[30] A.M. Awad, et al., Coenzyme Q_{10} deficiencies: pathways in yeast and humans, Essays Biochem. 62 (2018) 361–376.
[31] C.H. He, L.X. Xie, C.M. Allan, U.C. Tran, C.F. Clarke, Coenzyme Q supplementation or over-expression of the yeast Coq8 putative kinase stabilizes multi-subunit Coq polypeptide complexes in yeast coq null mutants, Biochim. Biophys. Acta 1841 (2014) 630–644.
[32] C. Ye, B.M. Sutter, Y. Wang, Z. Kuang, B.P. Tu, A metabolic function for phospholipid and histone methylation, Mol. Cell. 66 (2017) 180–193.E8.
[33] D.E. Vance, C.J. Walkey, L.B. Agellon, Why has phosphatidylethanolamine *N*-methyltransferase survived in evolution? Biochem. Soc. Trans. 26 (1998) 337–340.
[34] N. Presa, et al., Vitamin E alleviates non-alcoholic fatty liver disease in phosphatidylethanolamine *N*-methyltransferase deficient mice, Biochim. Biophys. Acta (BBA) - Mol. Basis Dis. 1865 (2019) 14–25.
[35] P.H. Pritchard, P.K. Chiang, G.L. Cantoni, D.E. Vance, Inhibition of phosphatidylethanolamine N-methylation by 3-deazaadenosine stimulates the synthesis of phosphatidylcholine via the CDP-choline pathway, J. Biol. Chem. 257 (1982) 6362–6367.
[36] C.J. Walkey, L.R. Donohue, R. Bronson, L.B. Agellon, D.E. Vance, Disruption of the murine gene encoding phosphatidylethanolamine *N*-methyltransferase, Proc. Natl. Acad. Sci. U.S.A. 94 (1997) 12880–12885.
[37] G. Hörl, et al., Sequential synthesis and methylation of phosphatidylethanolamine promote lipid droplet biosynthesis and stability in tissue culture and *in vivo*, J. Biol. Chem. 286 (2011) 17338–17350.
[38] L.M. Stead, J.T. Brosnan, M.E. Brosnan, D.E. Vance, R.L. Jacobs, Is it time to reevaluate methyl balance in humans? Am. J. Clin. Nutr. 83 (2006) 5–10.
[39] S.H. Mudd, et al., Methyl balance and transmethylation fluxes in humans, Am. J. Clin. Nutr. 85 (2007) 19–25.
[40] S. Fu, et al., Aberrant lipid metabolism disrupts calcium homeostasis causing liver endoplasmic reticulum stress in obesity, Nature 473 (2011) 528–531.
[41] K.L. Hoehn, et al., Insulin resistance is a cellular antioxidant defense mechanism, Proc. Natl. Acad. Sci. U.S.A. 106 (2009) 17787–17792.
[42] D.J. Fazakerley, et al., Mitochondrial oxidative stress causes insulin resistance without disrupting oxidative phosphorylation, J. Biol. Chem. 293 (2018) 7315–7328.
[43] K.L. Hoehn, et al., IRS1-independent defects define major nodes of insulin resistance, Cell Metab. 7 (2008) 421–433.
[44] U. Forsman, M. Sjöberg, M. Turunen, P.J. Sindelar, 4-Nitrobenzoate inhibits coenzyme Q biosynthesis in mammalian cell cultures, Nat. Chem. Biol. 6 (2010) 515–517.
[45] J.A. Stefely, et al., Mitochondrial protein functions elucidated by multi-omic mass spectrometry profiling, Nat. Biotechnol. 34 (2016) 1191–1197.

[46] M.D. Robinson, J. Grigull, N. Mohammad, T.R. Hughes, FunSpec: a web-based cluster interpreter for yeast, BMC Bioinf. 3 (2002) 35.
[47] Y. Tatsuta, et al., Imaging mass spectrometry analysis of ubiquinol localization in the mouse brain following short-term administration, Sci. Rep. 7 (2017) 12990.
[48] J.N. van der Veen, et al., The critical role of phosphatidylcholine and phosphatidylethanolamine metabolism in health and disease, Biochim. Biophys. Acta Biomembr. 1859 (2017) 1558–1572.
[49] J. Song, et al., Polymorphism of the PEMT gene and susceptibility to nonalcoholic fatty liver disease (NAFLD), FASEB J. 19 (2005) 1266–1271.
[50] J.E. Vance, Phospholipid synthesis in a membrane fraction associated with mitochondria, J. Biol. Chem. 265 (1990) 7248–7256.
[51] C. Kwak, et al., Contact-ID, a tool for profiling organelle contact sites, reveals regulatory proteins of mitochondrial-associated membrane formation, Proc. Natl. Acad. Sci. U.S.A. 117 (2020) 12109–12120.
[52] B.J. Floyd, et al., Mitochondrial protein interaction mapping identifies regulators of respiratory chain function, Mol. Cell. 63 (2016) 621–632.
[53] D.C. Lohman, et al., Mitochondrial COQ9 is a lipid-binding protein that associates with COQ7 to enable coenzyme Q biosynthesis, Proc. Natl. Acad. Sci. U.S.A. 111 (2014) E4697–E4705.
[54] M. Eisenberg-Bord, et al., The endoplasmic reticulum-mitochondria encounter structure complex coordinates coenzyme Q biosynthesis, Contact 2 (2019), 2515256418825409.
[55] K. Subramanian, et al., Coenzyme Q biosynthetic proteins assemble in a substrate-dependent manner into domains at ER-mitochondria contacts, J. Cell Biol. 218 (2019) 1353–1369.
[56] E. Tubbs, et al., Disruption of mitochondria-associated endoplasmic reticulum membrane (MAM) integrity contributes to muscle insulin resistance in mice and humans, Diabetes 67 (2018) 636–650.

Supplementary Information (SI) for Manuscript: *Genetic screening reveals phospholipid metabolism as a key regulator of the biosynthesis of the redox-active lipid coenzyme Q*

Anita Ayer[a,b], Daniel J. Fazakerley[c,d], Cacang Suarna[a,b], Ghassan J. Maghzal[b], Diba Sheipouri[b], Kevin J. Lee[b], Michelle C. Bradley[e], Lucía Fernández-del-Rio[e], Sergey Tumanov[a,b], Stephanie MY Kong[a,b], Jelske N. van der Veen[f], Andrian Yang,[b,g], Joshua W.K. Ho[b,g,h,i], Steven G. Clarke[e], David E. James[c], Ian W. Dawes[j], Dennis E. Vance[k], Catherine F. Clarke[e], René L. Jacobs[f] and Roland Stocker[a,b,g,l]*

Affiliations:

[a]Heart Research Institute, The University of Sydney; Sydney, New South Wales, Australia
[b]Victor Chang Cardiac Research Institute; Sydney, Australia
[c]Charles Perkins Centre, School of Life and Environmental Sciences, Sydney Medical School, The University of Sydney; Sydney, Australia
[d]Metabolic Research Laboratory, Wellcome-Medical Research Council Institute of Metabolic Science, University of Cambridge; Cambridge, United Kingdom
[e]Department of Chemistry and Biochemistry, and the Molecular Biology Institute, University of California; Los Angeles, United States
[f]Department of Agricultural, Food and Nutritional Science, University of Alberta; Edmonton, Canada
[g]St Vincent's Clinical School, University of New South Wales, Sydney, Australia
[h]School of Biomedical Sciences, Li Ka Shing Faculty of Medicine, University of Hong Kong, Hong Kong SAR, China
[i]Laboratory for Data Discovery for Health, Hong Kong Science Park, Hong Kong SAR, China
[j]School of Biotechnology and Biomolecular Sciences, University of New South Wales; Sydney, Australia
[k]Department of Biochemistry, University of Alberta; Edmonton, Canada
[l]School of Life and Environmental Sciences, The University of Sydney, Sydney, Australia

***Corresponding author: Roland Stocker**
Address: Heart Research Institute, 7 Eliza St Newtown, Australia 2042
Email: roland.stocker@hri.org.au

This PDF file includes:

Table S2. Genotype and source of yeast strains

Strain	Genotype	Source
BY4743	*MAT***a**/*MATα his3Δ1/his3Δ1 leu2Δ0/leu2Δ0 LYS2/lys2Δ0 met15Δ0/MET15 ura3Δ0/ura3Δ0*	(1)
Homozygous diploid strains	*MAT***a**/*MATα his3Δ1/his3Δ1 leu2Δ0/leu2Δ0 LYS2/lys2Δ0 met15Δ0/MET15 ura3Δ0/ura3Δ0 Gene of interest::KanMX*	(2)
BY4743 *CHO2* heterozygous	*MATα his3Δ1 leu2Δ0 lys2Δ0 ura3Δ0; MATa his3Δ1 leu2Δ0 met15Δ0 ura3Δ0 CHO2::KanMX*	This study
BY4743 rho^0	*MAT***a**/*MATα his3Δ1/his3Δ1 leu2Δ0/leu2Δ0 LYS2/lys2Δ0 met15Δ0/MET15 ura3Δ0/ura3Δ0; respiratory incompetent*	This study
BY4742	*MATα his3Δ1 leu2Δ0 lys2Δ0 ura3Δ0*	
BY4741	*MAT**a** his3Δ1 leu2Δ0 met15Δ0 ura3Δ0*	R. Yang
BY4741 *cho2Δ*	*MAT**a** his3Δ1 leu2Δ0 met15Δ0 ura3Δ0 CHO2::KanMX*	R. Yang
BY4741 *ste14Δ*	*MAT**a** his3Δ1 leu2Δ0 met15Δ0 ura3Δ0 STE14::KanMX*	R. Yang
BY4742 *coq1*Δ	*MATα his3Δ0 leu2Δ0 met15Δ0 ura3Δ0 COQ1::KanMX4*	(2)
BY4742 *coq3*Δ	*MATα his3Δ0 leu2Δ0 met15Δ0 ura3Δ0 COQ 3::KanMX4*	(2)
BY4742 *coq4*Δ	*MATα his3Δ0 leu2Δ0 met15Δ0 ura3Δ0 COQ 4::KanMX4*	(2)
BY4742 *coq5*Δ	*MATα his3Δ0 leu2Δ0 met15Δ0 ura3Δ0 COQ 5:: KanMX4*	(2)
BY4741*coq6*Δ	*MATα his3Δ0 leu2Δ0 met15Δ0 ura3Δ0 COQ 6::KanMX4*	(2)
BY4742 *coq7*Δ	*MATα his3Δ0 leu2Δ0 met15Δ0 ura3Δ0 COQ 7::KanMX4*	(2)
BY4742 *coq8*Δ	*MATα his3Δ0 leu2Δ0 met15Δ0 ura3Δ0 COQ::KanMX4*	(2)
BY4742 *coq9*Δ	*MATα his3Δ0 leu2Δ0 met15Δ0 ura3Δ0 COQ9::KanMX4*	(2)
BY4742 *coq10*Δ	*MATα his3Δ0 leu2Δ0 met15Δ0 ura3Δ0 COQ10::KanMX4*	(2)
BY4742 *coq11*Δ	*MATα his3Δ0 leu2Δ0 met15Δ0 ura3Δ0 coq11::LEU2*	(3)
W303-1a	*MATa leu2-3,112 trp1-1 can1-100 ura3-1 ade2-1 his3-11,15*	A. Cooper
W303-1a *cho2Δ*	*MAT**a** leu2-3,112 trp1-1 can1-100 ura3-1 ade2-1 his3-11,15 CHO2::NatMX*	This study

Table S3. Primers used in this study

Name	Primer sequence (5'-3')	Source
CHO2-S1	TTTCGAGTGATTTTCTTAGTGACAAAGC TTTTTCTTCATCTGTAGATGCGTACGCTG CAGGTCGAC	This study
CHO2-S2	GAATCCTAGTACTTTTTAAATATATATA CTCAAAAAAAAAAAACTCAATCGATGA ATTCGAGCTCG	This study
CHO2-A	ATACAGATTCTTTCCACTGTGTTCC	(4)
CHO2-D	GCTGTTTAATGAACCAGGAAACTTA	(4)
CHO2-F	GTGATATTATTGACACGCCCATGTCCAG TTGTAAAACC	This study
CHO2-R	GGGATCACCATCCGTCGCCCTCAAGCAA GACTATCAAG	This study
mtDNA F	GTGCGTATATTTCGTTGATGCGT	(5)
mtDNA R	TTCACACTGCCTGTGCTATCTAA	(5)
yACT1F	TATGTTCTAGCGCTTGCACCA	This study
yACT1R	CCAAAGCAGCAACCTCTAAA	This study
yCOQ1F	CCCGAAGTCGTAGAACTAATG	This study
yCOQ1R	GGAACCGGAAGTAGCTTATG	This study
yCOQ2F	CAGCTGGTATGTTGGGTATTT	This study
yCOQ2R	GACGGACCTGATAACTCTTTG	This study
yCOQ3F	CATGCTGGAGGGAAAGATAAA	This study
yCOQ3R	TCGACCAACAATGCCTTAAA	This study
yCOQ4F	GTGGTATCCTTGCACCTTTAC	This study
yCOQ4R	CCAGCATTTCCTCCCAATAC	This study
yCOQ5F	TGCTTAAAGAAGGTGAGAAGAG	This study
yCOQ5R	TACCGAAGGAGACTGTGTAG	This study
yCOQ6F	TGAAGGACGAGTCGGATATT	This study
yCOQ6R	CCAACAAGGGCAACTCTATC	This study
yCOQ7F	GCTCCCAAGTGTCAGAATTTA	This study
yCOQ7R	CTGGTCCCATATGTGCTTTAG	This study
yCOQ8F	CGTATGGAGGGAACTGAAATAA	This study
yCOQ8R	GAGGCACCGAAATCCAATAA	This study
yCOQ9F	CGCTGTCATGGAACTGATAAA	This study
yCOQ9R	GAGAAAGGCGCTTGGAATAG	This study
yCOQ10F	GCGGTACCAATCACACTATTA	This study
yCOQ10R	GAGAGGCTTGTTATCCACAG	This study
yCOQ11F	GCAGAGATATTTCAGGCCTATTA	This study
yCOQ11R	CTGCTGAGTGGATACTGTTG	This study
mPDSS1F	ACACCAGCAATGTGCAGTTG	This study
mPDSS1R	ACAGACCTTTCAAGTCTCTCCAG	This study
mPDSS2F	CGCTTGTCCGGTTACCTCG	This study
mPDSS2R	GGGTAGCCCACGATCTTCTC	This study
mCOQ2F	ACAAGCCCATAGGAACCTGG	This study
mCOQ2R	CTCCACGCATCAGAATAGCTC	This study
mCOQ3F	CTCGTGGGGTTCGTCTCCT	This study
mCOQ3R	GAGCTGCGTCCCTGAGTAAG	This study
mCOQ4F	TGTACCCGGACCACATCCC	This study
mCOQ4R	AACCATGTCGTGGCGATAGG	This study
mCOQ5F	CCCAGGTGCTGCGTTCTATG	This study
mCOQ5R	GTCTCAAACCCGAAGTGCG	This study
mCOQ6F	CTCAGCAGTTTTGGTGCATGG	This study

mCOQ6R	TGTCCCTGTCGAACATTATCAAG	This study
mCOQ7F	ACGAGTTGATGATTGCATTCAGG	This study
mCOQ7R	TTCCCCAGCAAGGCAGTTC	This study
mCOQ8F	CCATTGGGCAGGTACACCAAG	This study
mCOQ8R	CTCTGCGGTAGTCACATTCCC	This study
mCOQ9F	GTGGGGTTCCGGTCTTCAG	This study
mCOQ9R	GGGGTGGACGGGAAAACTC	This study
mCOQ10F	CAGCTCGGACCAGTCAGAG	This study
mCOQ10R	TCCTCCATTCCTGATACTACGTC	This study
mβACTF	GGATGCAGAAGGAGATCACTG	(6)
mβACTR	CGATCCACACGGAGTACTTG	(6)
mCYCBF	TTCTTCATAACCACAGTCAAGACC	(7)
mCYCBR	ACCTTCCGTACCACATCCAT	(7)
mPEMTF	TGGCTGCTGGGTTACATGG	This study
mPEMTR	GCTTCCGAGTTCTCTGCTCC	This study

Table S4 –Antibody list

Antibody	*Working dilution*	*Source*
Coq1	1:10,000	(8)
Coq2	1:1,000	(9)
Coq3	1:200	(10)
Coq4	1:2,000	(11)
Coq5	1:5,000	(12)
Coq6	1:200	(13)
Coq7	1:1,000	(14)
Coq8	Affinity purified, 1:30	(15)
Coq9	1:1,000	(15)
Coq10	Affinity purified, 1:400	(16)
Coq11	1:500	(16)
Mdh1	1:10,000	Lee McAlister-Henn[a]
Porin (459500)	1:1000	Thermo Fisher Scientific
Tubulin (MAB1501)	1:1000	MP Biomedicals

[a]Dr. Lee McAlister-Henn, Department of Molecular Biophysics and Biochemistry, University of Texas Health Sciences Center, San Antonio, TX

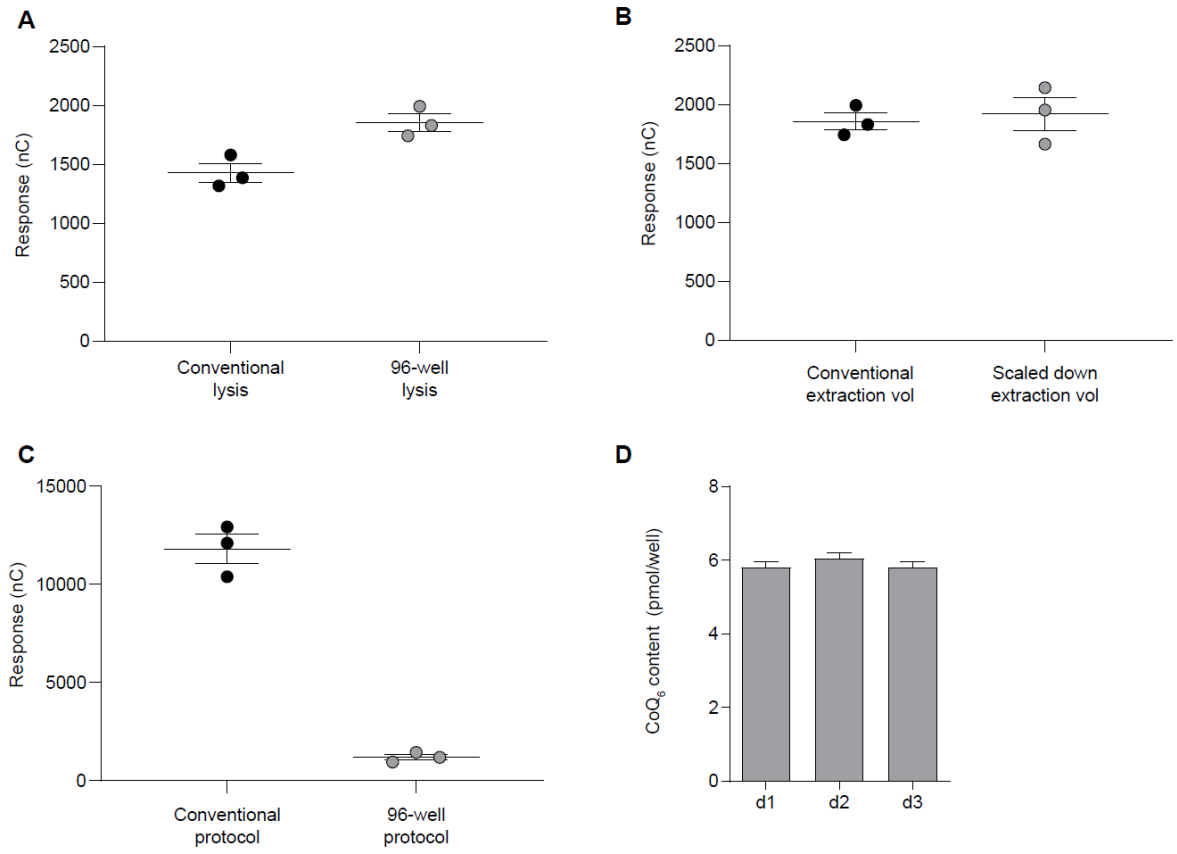

Fig. S1. Development and validation of a 96-well plate method for cell growth, lysis and CoQ extraction of yeast cells. (A) HPLC-ECD analyses of CoQ content in cells lysed either using the conventional process (fast prep) or in a 96-well plate. **(B)** HPLC-ECD analyses of CoQ content in cells extracted either using the conventional volumes of hexane/methanol (12 mL) or scaled down reagent volumes (2.5 mL). **(C)** Comparison of HPLC-ECD response from cells grown, lysed and extracted in the conventional manner versus cells grown, lysed and extracted in a 96-well plate. **(D)** Inter- and intraday reproducibility of cells grown, lysed and extracted in a 96-well plate. Data and error bars depict mean ± s.e.m.

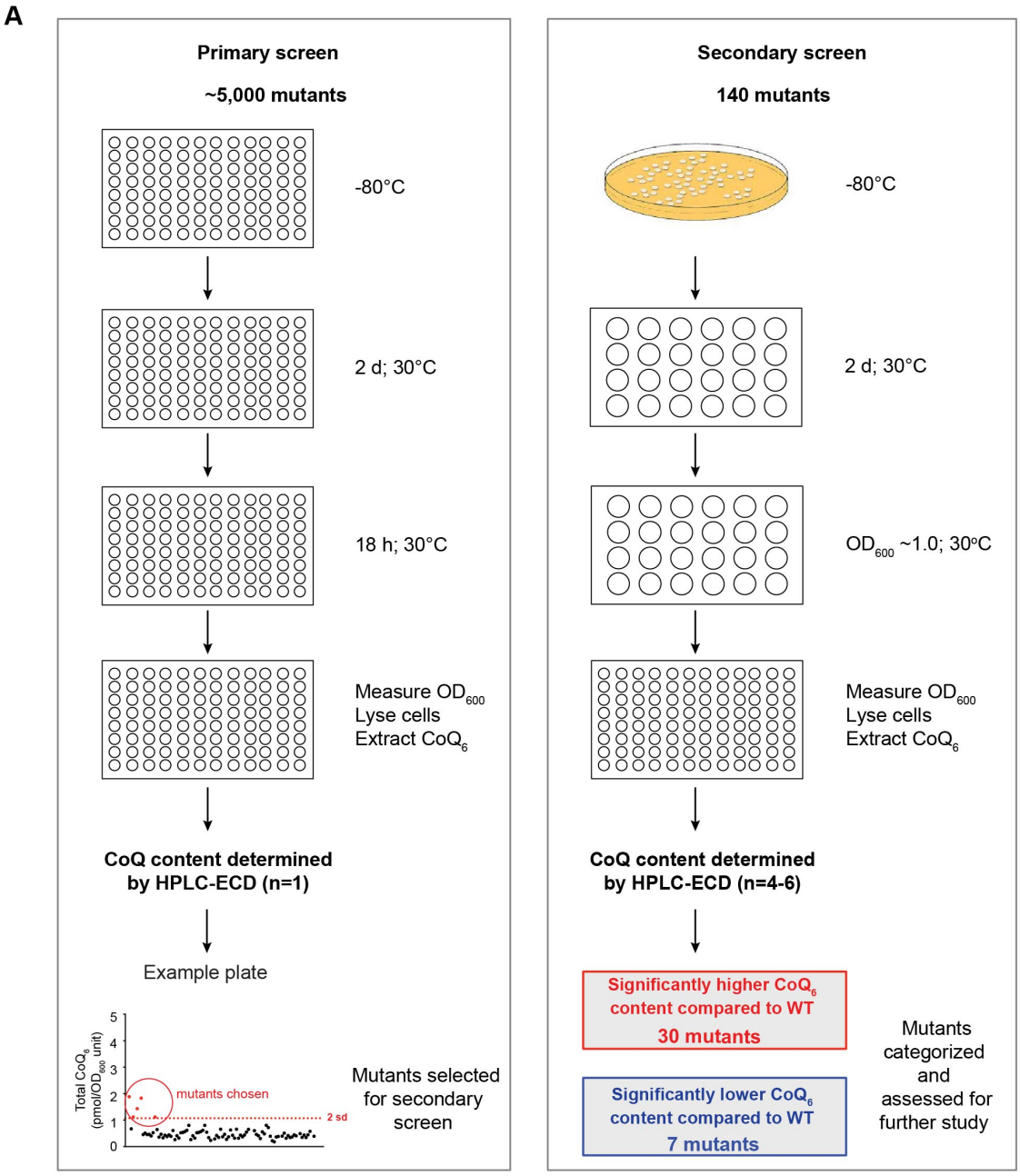

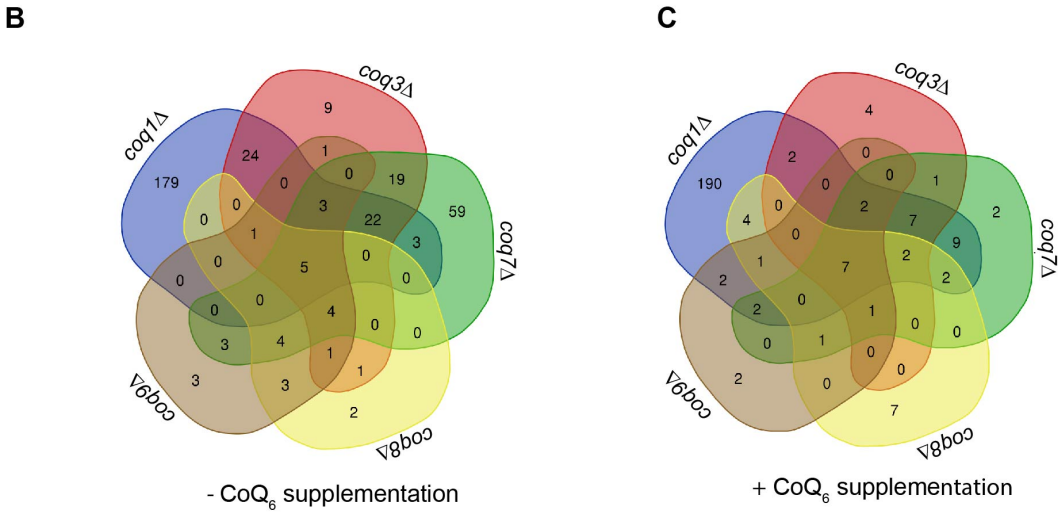

Fig. S2. Schematic representation of the experimental workflow of genetic screen and microarray results. (**A**) *Primary screen:* Frozen stocks of the homozygous diploid yeast knockout collection were thawed, replica plated into 96-well plates containing synthetic defined media lacking CoQ head group

precursors (SD minus 4HB-pABA) and grown for 2 d at 30 °C. Cells were replica plated into fresh SD minus 4HB-pABA in 96-well plates, grown for 18 h at 30 °C and OD_{600} measured before lysis and CoQ_6 extracted. CoQ_6 in each mutant was determined by HPLC-ECD, normalized to biomass and the average CoQ_6 content of mutants on each plate calculated. Mutants with CoQ_6 content two standard deviations above or below the plate population mean were selected for secondary screening. *Secondary screen:* WT BY4743 and selected mutants were recovered from -80 °C glycerol stocks, grown on YEPD agar plates for 2 d at 30 °C, and inoculated into 24-well plates containing SD minus 4HB-pABA for 2 d at 30 °C. Cells were subsequently inoculated into 24-well plates containing SD minus 4HB-pABA and grown at 30 °C to exponential phase ($OD_{600\ nm}$ ~1.0). Cells were lysed, CoQ_6 content in each mutant determined by HPLC-ECD and normalized to biomass. Mutants with significantly higher or lower CoQ_6 content compared to WT were identified for further study. **B-C**) Venn diagram of differentially expressed genes in different *coq* mutants grown in the absence (**B**) or presence (**C**) of CoQ_6 supplementation Abbreviations: 4-HB, 4-hydroxybenzoic acid; CoQ, coenzyme Q; HPLC-ECD, high-performance liquid chromatography-electrochemical detection; OD_{600}, optical density at 600 nm; pABA, *para*-aminobenzoic acid; YEPD, yeast extract peptone dextrose.

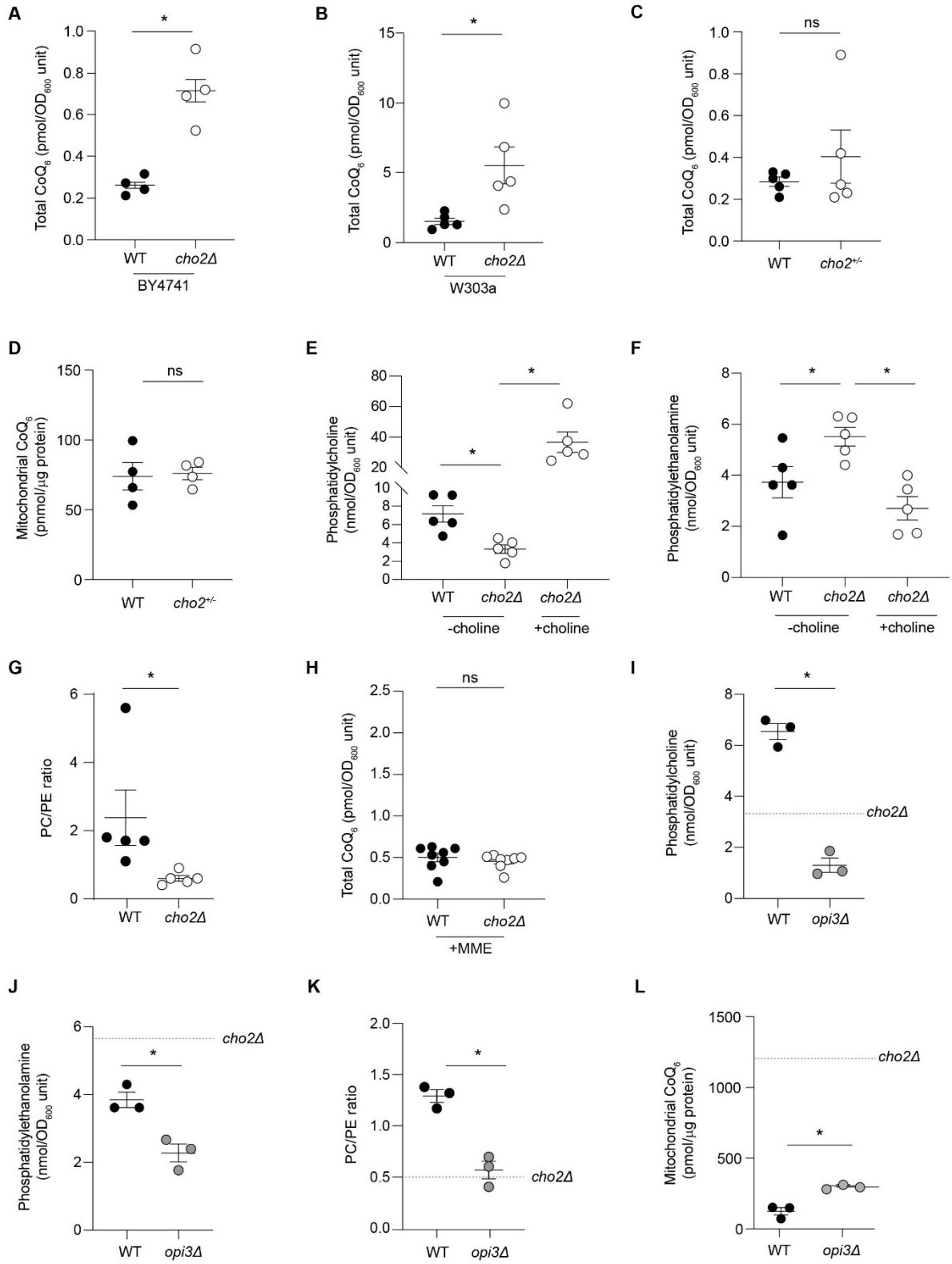

Fig. S3. Deletion of the *CHO2* gene results in increased cellular CoQ_6 content that is independent of phosphatidylcholine concentrations in *S. cerevisiae*. **(A)** Concentration of CoQ_6 in haploid WT and *CHO2* deficient mutants in the BY4741 genetic background (n=4). **(B)** Concentration of CoQ_6 in haploid WT and *CHO2*-deficient mutants in the W303a genetic background (n=5). **(C)** Total CoQ_6 content in WT and yeast cells heterozygous for *CHO2* in the BY4743 background (n=5). **(D)** Mitochondrial CoQ_6 content in WT and yeast cells heterozygous for *CHO2* in the BY4743 background (n=4). **(E)** Phosphatidylcholine concentrations in WT and *cho2Δ* mutants with and without 1 mM choline supplementation (n=5). **(F)** Phosphatidylethanolamine concentrations in WT and *cho2Δ* mutants with and without 1 mM choline supplementation (n=5). **(G)** PC/PE ratio in WT and *cho2Δ* mutants (n=5). **(H)** CoQ_6 concentrations in WT and *cho2Δ* mutants with and without 1 mM monomethylethanolamine (MME) supplementation (n=8). (I) Phosphatidylcholine concentrations in

WT and *opi3Δ* mutants (n=3). **(J)** Phosphatidylethanolamine concentrations in WT and *opi3Δ* mutants (n=3). **(K)** PC/PE in ratio in WT and *opi3Δ* mutants (n=3). **(L)** Mitochondrial CoQ_6 content in WT cells and *opi3Δ* mutants (n=3). For panels **I-L**, dashed lined represents the mean value observed in *cho2Δ* mutants. Data and error bars depict mean ± s.e.m. *P ≤ 0.05 and ns indicates 'not significant' as determined by Mann-Whitney test.

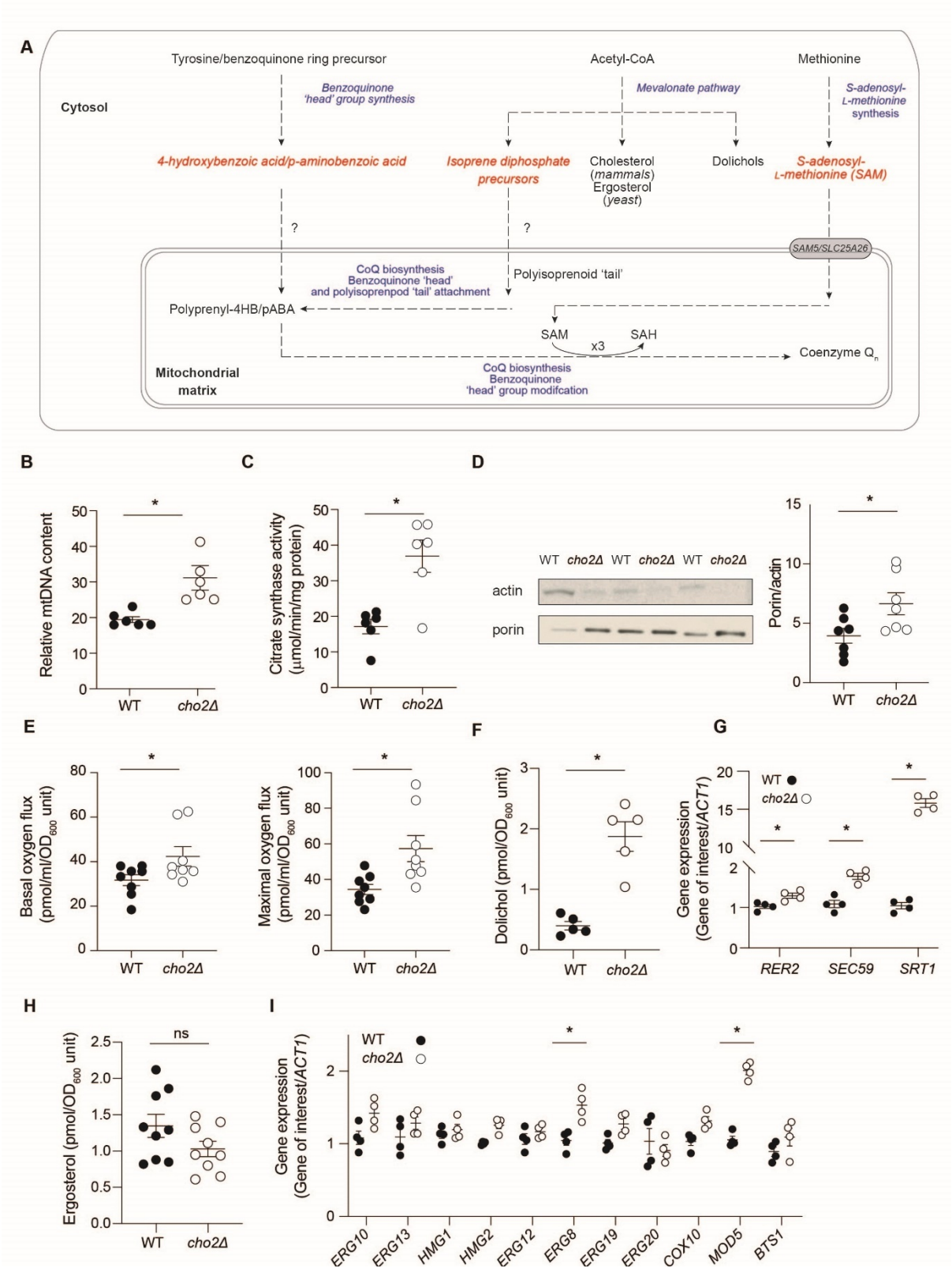

Fig. S4. Increased CoQ_6 in *cho2Δ* cannot be explained by changes in mitochondrial mass or changes in the mevalonate pathway in *S. cerevisiae*. (**A**) Schematic outlining the biochemical pathways involved in CoQ biosynthesis and their cellular localization. Question marks indicate pathways currently not elucidated. (**B-D**) *cho2Δ* mutant have increased mitochondrial mass compared with WT cells (n=6-7) as indicated by increased: mitochondrial DNA content determined by quantitative PCR (**B**), citrate synthase activity (**C**) and porin content determined by Western blotting (**D**). (**E**) Basal and maximal respiration rates in WT and *cho2Δ* mutants as measured by high-resolution respirometry (n=8). (**F**) Dolichol concentration in WT and *cho2Δ* mutants as measured by LC/MS/MS (n=5). (**G**) Gene expression of dolichol synthesis pathway in *cho2Δ* mutants compared to WT determined by qPCR (n=4). (**H**) Ergosterol concentration in WT and *cho2Δ* mutants as measured by

HPLC-UV (n=9). (**I**) Mevalonate pathway gene expression in *cho2Δ* mutants compared to WT determined by qPCR (n=4). Data and error bars depict mean ± s.e.m. *$P \leq 0.05$ and ns indicates 'not significant' as determined by Mann-Whitney test (**B-F, H**) or by 2-way ANOVA with Sidak's multiple comparison test (**G, I**).

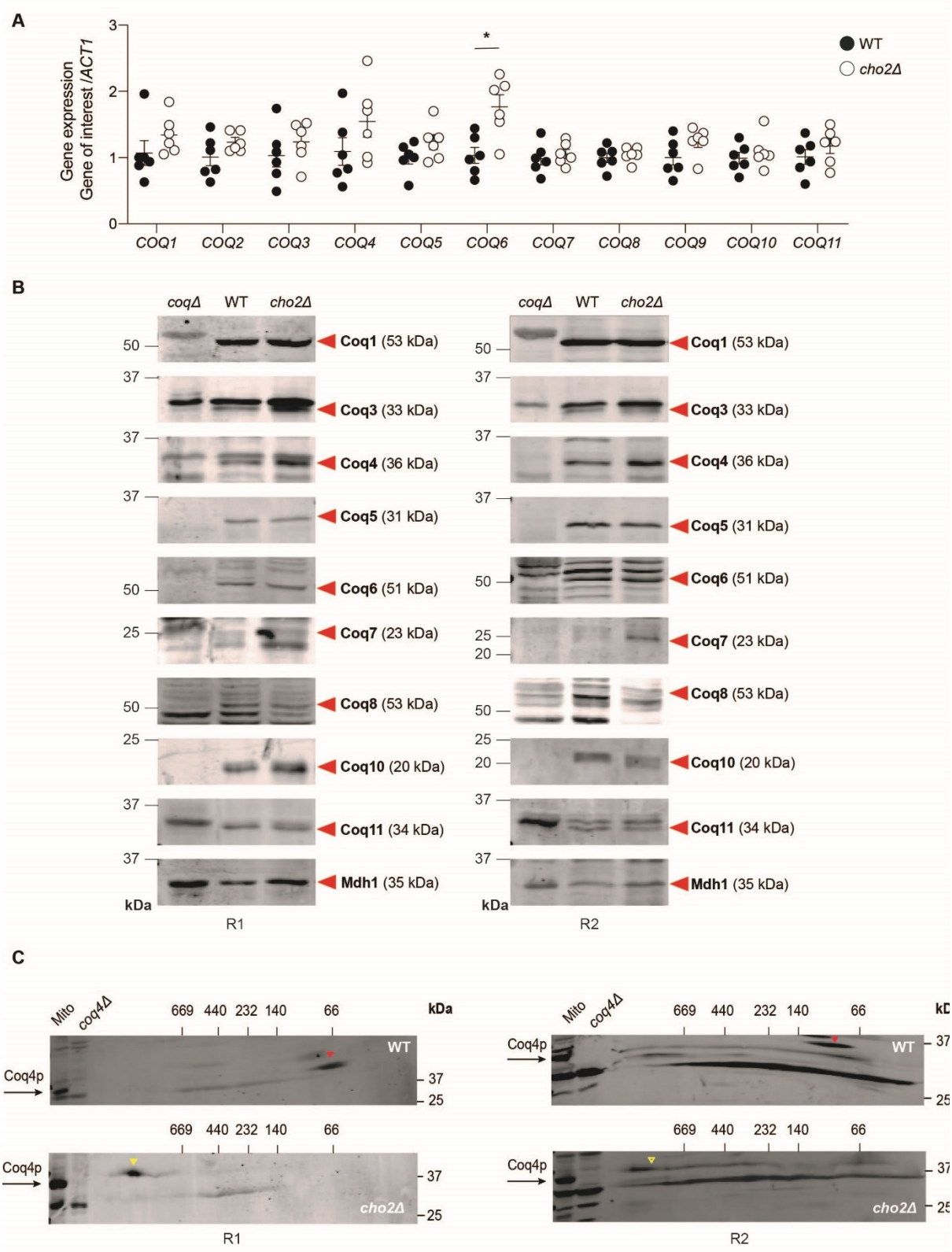

Fig. S5. Increased CoQ_6 in *cho2Δ* cannot be explained by changes in the expression of the CoQ biosynthetic pathway. (**A**) Gene expression of the CoQ biosynthetic genes in *cho2Δ* mutants compared to WT as determined by qPCR (n=6). (**B**) Protein levels of the CoQ biosynthetic pathway in isolated mitochondria from WT and *cho2Δ* as measured by Western blotting (n=3), representative image shown. (**C**) Two-dimensional Blue Native/SDS PAGE separation and immunoblotting of the high molecular weight CoQ synthome protein complex in WT and *cho2Δ*. (n=3), representative image shown. Red arrow indicates low molecular mass species in WT and the yellow arrow indicates an increase in a high molecular weight species in *cho2Δ*. Data and error bars depict mean ± s.e.m. *P ≤ 0.05 as determined by Kruskal-Wallis test (**A**). **B** and **C** show results of two independent replicates (R1 and R2).

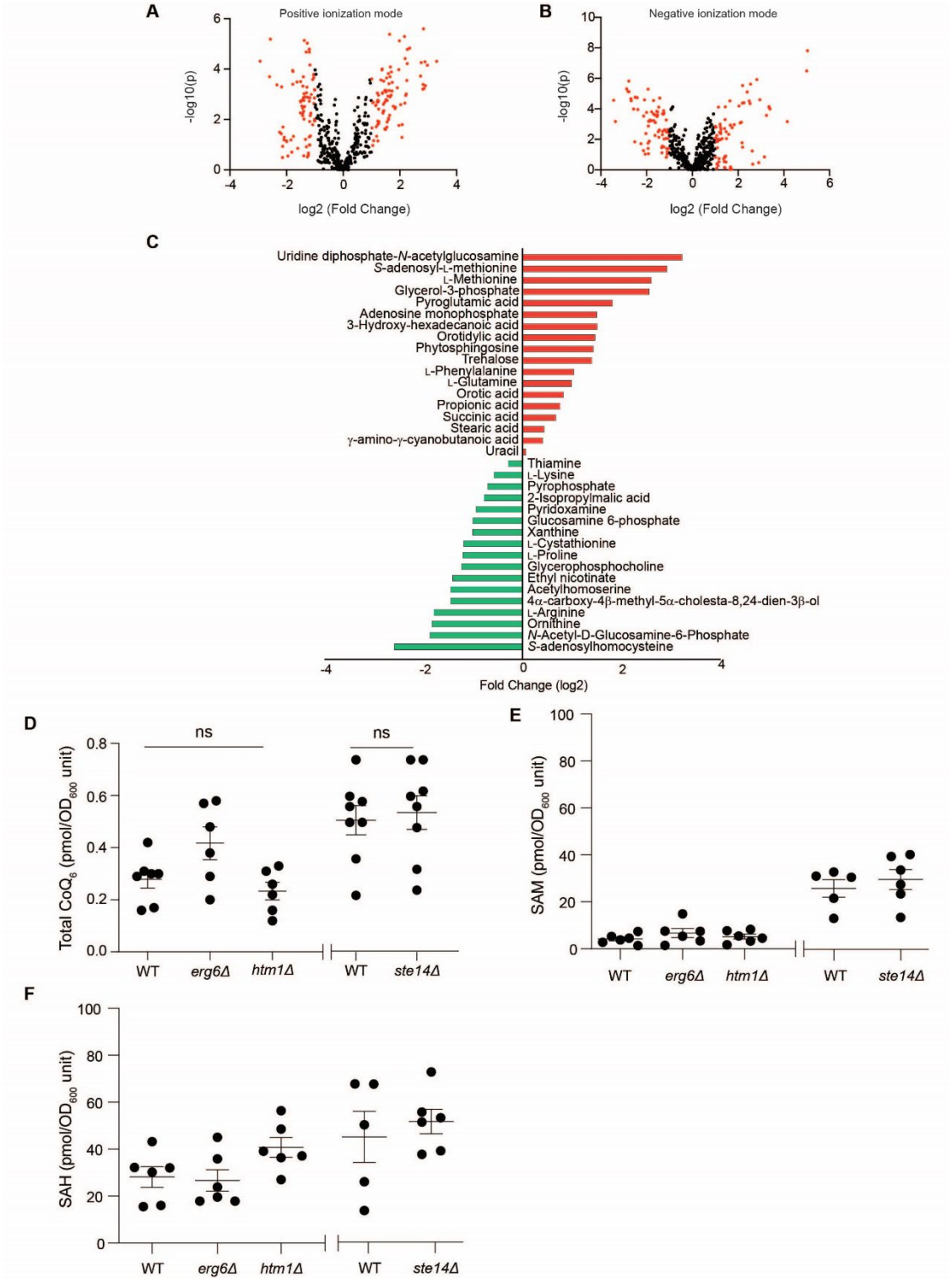

Fig. S6. Untargeted metabolomics analyses of WT and *cho2Δ* reveal *S*-adenosylmethionine (SAM) and *S*-adenosylhomocysteine (SAH) alterations. (**A-B**), Volcano plots indicating significantly alerted metabolites (red) in *cho2Δ* versus WT cells in both positive and negative ionization modes. Data taken from n=5. (**C**) Metabolites significantly altered in *cho2Δ* versus WT cells. Data taken from n=5. (**D**) CoQ_6 content in yeast methyltransferase mutants *erg6Δ, htm1Δ* and *ste14Δ* (n=6). (**E**) SAM content in yeast methyltransferase mutants *erg6Δ, htm1Δ* and *ste14Δ* versus their respective WT cells (n=6). (**F**) SAH content in yeast methyltransferase mutants *erg6Δ, htm1Δ* and *ste14Δ* versus their respective WT cells (n=6). The *erg6Δ* and *htm1Δ* strains were in the BY4743 background and compared to BY4743 WT for all studies. The *ste14Δ* used was in the BY4741 background and compared to BY4741 WT for all studies. Data and error bars in **D-F** depict mean ± s.e.m. *P ≤ 0.05 and ns indicates 'not significant' as determined by Mann-Whitney (*ste14Δ*) or Kruskal-Wallis test (*erg6Δ* and *htm1Δ*).

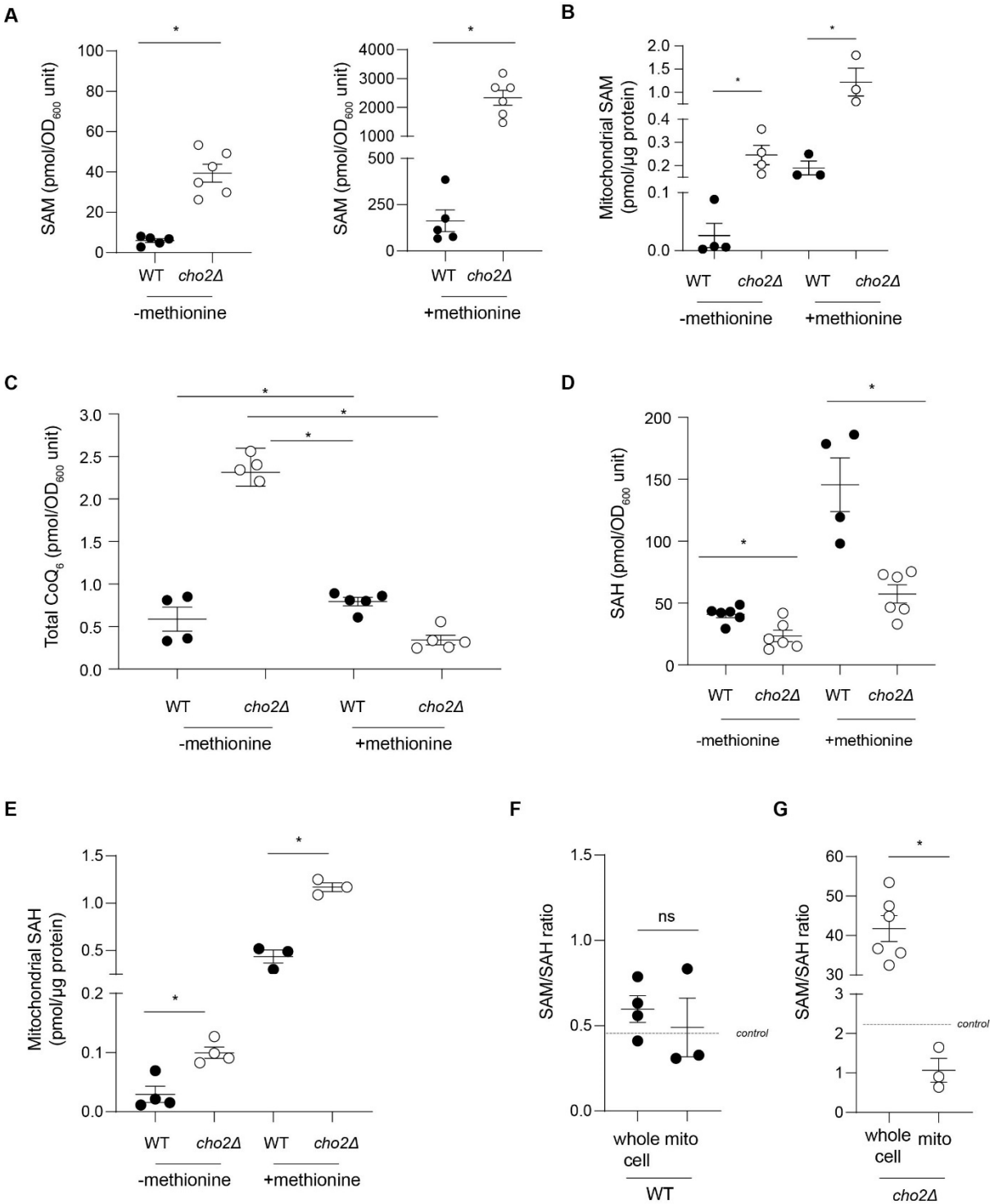

Fig. S7. Treatment with methionine drives changes in the mitochondrial SAM-to-SAH ratio in *S. cerevisiae*. (**A**) Whole-cell SAM content in WT and *cho2Δ* grown in the presence or absence of 1 mM methionine (n=3-4). (**B**) Mitochondrial SAM content in WT and *cho2Δ* grown in the presence or absence of 1 mM methionine (n=3)**.** (**C**) CoQ_6 content in WT and *cho2Δ* grown in the presence or absence of 1 mM methionine (n=4-5). (**D**) Whole-cell SAH content in WT and *cho2Δ* grown in the presence or absence of 1 mM methionine (n=3-4). (**E**) Mitochondrial SAH content in WT and *cho2Δ* grown in the presence or absence of 1 mM methionine (n=3). (**F**) Whole-cell and mitochondrial SAM/SAH ratios in WT cells treated with 1 mM methionine (n=3-4). (**G**) Whole-cell and mitochondrial SAM/SAH ratios in *cho2Δ* cells treated with 1 mM methionine (n=3-4). In **E** and **G**, dotted line represents untreated (control) values of respective strains. Data and error bars depict mean ± s.e.m. *P ≤ 0.05 and ns indicates 'not significant' as determined by Mann-Whitney (**F-G**) or Kruskal-Wallis test (**A-E**).

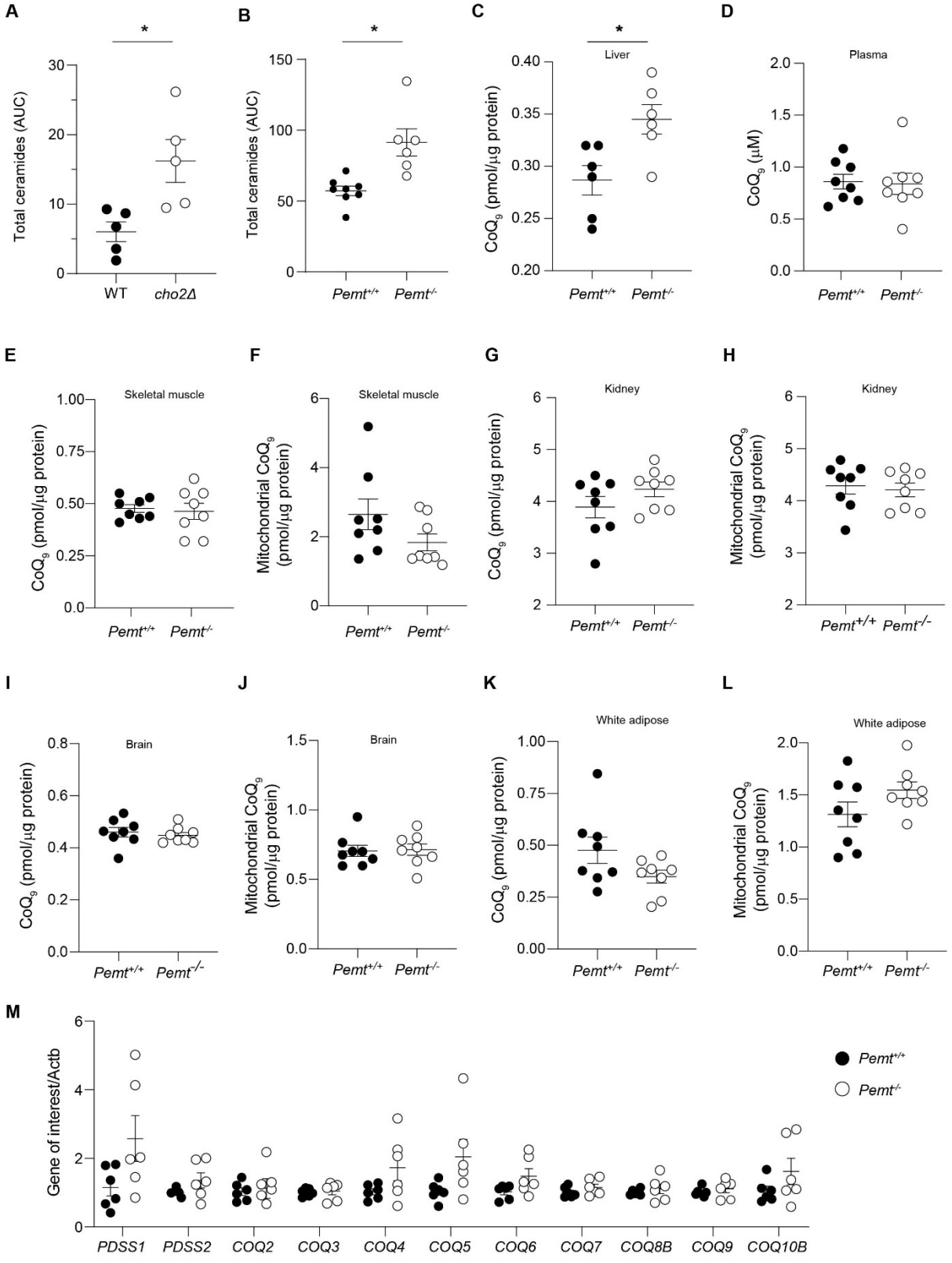

Fig. S8. Pemt deficiency selectively increases liver CoQ in mice fed chow diet. (**A**) Total ceramide species in WT and *cho2Δ*. **(B)** Total hepatic ceramide species in $Pemt^{+/+}$ and $Pemt^{-/-}$ mice. **(C)** Total hepatic CoQ_9 content in $Pemt^{+/+}$ and $Pemt^{-/-}$ mice fed chow (n=6). (**D**) Plasma CoQ_9 content in $Pemt^{+/+}$ and $Pemt^{-/-}$ mice fed chow (n=8). (**E-F**) Total and mitochondrial CoQ_9 content in skeletal muscle (n=8). (**G-H**) Total and mitochondrial CoQ_9 content in kidney (n=8). (**I-J**), Total and mitochondrial CoQ_9 content in brain (n=8). (**K-L**) Total and mitochondrial CoQ_9 content in white adipose tissue (n=8). (**M**) Hepatic gene expression of the CoQ biosynthetic pathway in $Pemt^{+/+}$ and $Pemt^{-/-}$ mice fed chow as determined by qPCR (n=6). Data and error bars depict mean ± s.e.m. $*P \leq 0.05$ as determined by Mann-Whitney (**A-J**) or Kruskal-Wallis test (**K**).

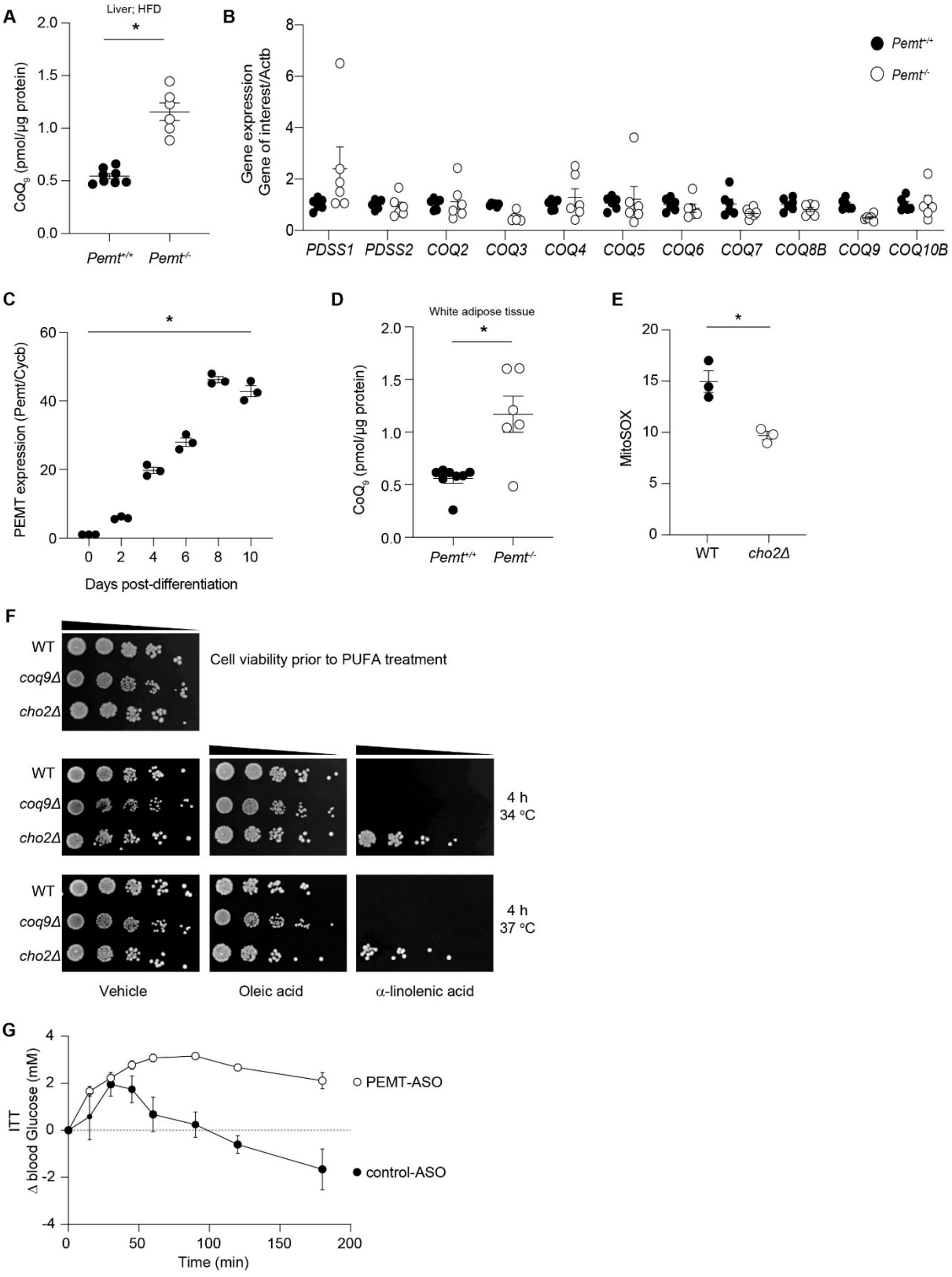

Figure S9. Pemt deficiency in mice fed a high-fat diet (HFD) and effect on mitochondrial superoxide production. (**A**) Total hepatic CoQ_9 content in *Pemt*$^{+/+}$ and *Pemt*$^{-/-}$ mice a HFD for 6 weeks (n=6-8). (**B**) Hepatic gene expression of the CoQ biosynthetic pathway in *Pemt*$^{+/+}$ and *Pemt*$^{-/-}$ mice fed HFD for 6 weeks as determined by qPCR (n=6). (**C**) PEMT gene expression as measured by qPCR during differentiation in 3T3-L1 adipocytes (n=3). (**D**) Total CoQ_9 content in white adipose tissue in *Pemt*$^{+/+}$ and *Pemt*$^{-/-}$ mice fed HFD for 6 weeks (n=6-8). (**E**) Mitochondrial superoxide content in *cho2Δ* compared to WT cells as measured by MitoSOX fluorescence (n=3)**.** (**F**) Polyunsaturated fatty acid stress assay induced by α-linolenic acid at elevated temperatures in WT and *cho2Δ*. Oleic acid was used as a monounsaturated fatty acid control, and *coq9Δ* as a CoQ deficient control strain. Representative image of three independent replicates shown. **(G)**

Baseline (0 min) corrected blood glucose concentrations (Δ blood glucose) in C57BL/6J mice fed HFD treated with either control or anti-PEMT ASO for 10 weeks. Δ blood glucose concentrations were determined over three hours post insulin challenge with inversed values plotted. Dotted line indicates baseline. Data is mean of n=5-10 mice per group. Data and error bars depict mean ± s.e.m. $*P \leq 0.05$ as determined by Mann-Whitney (**A, D, E**) or Kruskal-Wallis test (**B, C**).

Materials and Methods

Methods

Yeast strains

See Table S2 for details of *Saccharomyces cerevisiae* (*S. cerevisiae*) strains used in this study. For the genome-wide screen and subsequent experiments, *S. cerevisiae* homozygous diploid BY4743 WT and corresponding knockout mutants were used. For selected experiments where haploid yeast strains were required, yeast from the BY4741 or W303a backgrounds were used. BY4743 *CHO2* heterozygous diploid strain was constructed by crossing BY4741 *cho2Δ* with BY4742 WT using standard yeast techniques (17). *CHO2* was disrupted in W3031a using a one-step gene replacement method using the nourseothricin antibiotic resistance cassette from *pFA6a*–natNT2 (18). For *CHO2* knockout (*CHO2*-S1 and *CHO2*-S2) and verification primers (*CHO2*-A and *CHO2*-D) see Table S3. Rho^0 strains were generated by growth of WT cells in medium containing 10 mg/mL ethidium bromide for two rounds of growth. Respiratory incompetence was verified by comparison of growth on media containing glucose (2% w/w) with medium containing glycerol (3% w/v). Cells that grew on glucose but not glycerol containing medium were considered respiratory incompetent.

Yeast cell growth

For all experiments, yeast cells were recovered from -80 °C glycerol stocks in YEPD liquid (2% glucose, 1% yeast extract, 2% peptone) or YEPD agar (YEPD plus 2% bacteriological agar) for 2 d at 30 °C. Subsequently, all growth was carried out in synthetic defined medium lacking the CoQ head-group precursors 4-hydroxybenzoic acid (4HB) and *para*-aminobenzoic acid (pABA) (SD-4HB-pABA; 2% glucose or galactose, 6.7% yeast nitrogen base + nitrogen lacking 4-hydroxybenzoic acid and *para*-aminobenzoic acid (Sunrise Scientific #1563-100)) supplemented with appropriate amino acids and bases (1.3% leucine, 0.9% lysine, 0.38% isoleucine, 0.60% valine, 0.23% histidine, 0.45% tryptophan, 0.275% adenine, 0.11% uracil (w/v)) unless otherwise indicated. Cells were grown at 30 °C with shaking until cell biomass reached OD_{600} ~1.0 or as indicated. Cell cultures were harvested by centrifugation (17,000 x *g*; 10 min; 4 °C) and cells were used immediately or stored at -20 °C until further use.

Construction of constitutive low-copy CHO2 yeast expression vector and expression in yeast

A constitutive low-copy *CHO2* containing plasmid was constructed using the pAG416-GPD vector backbone donated kindly by Prof. Anthony Cooper (Garvan Medical Research Institute). The *CHO2* open reading frame was cloned into pAG416-GPD using Gibson Assembly (New England Biolabs; see Table S3 for primers *CHO2*-F and *CHO2*-R). Clones were sequenced by Sanger sequencing, and positive clones were transformed into BY4743 WT and *cho2Δ* yeast,

along with the corresponding empty vector (pAG416-GPD) control using the lithium acetate method (19). Yeast cells were grown using media lacking uracil to maintain selection pressure.

Overexpression of mitochondrial-targeted SAM1 in yeast

Plasmids expressing cytosolic *SAM1* (SAM1-pYES2) and mitochondrial-targeted *SAM1* (Su9(1–69)-*SAM1*-pYES2) (20) were kindly donated by Dr. Agrimi (University of Bari). SAM1-pYES2 and Su9(1–69)-SAM1-pYES2 were transformed into BY4743 WT and *cho2*Δ yeast, along with the corresponding empty vector (pYES2) control using the Li-acetate transformation method (19). Yeast cells were grown using media lacking uracil to maintain selection pressure.

Transcriptomic analyses

Yeast cultures were grown overnight in SD-4HB-pABA. Pre-cultures were diluted and grown overnight with shaking (30 °C) until cell density reached OD_{600} ~1.0 in SD-4HB-pABA. For experiments involving CoQ_6 supplementation, cells were grown in the presence of 10 μM CoQ_6. Cell were harvested at OD_{600} ~1.0 cell pellets were store at -20 °C until analyses. RNA was extracted from cells using TRIzol reagent (Invitrogen) and DNA contamination was removed using the DNase TURBO kit as per manufacturer's instructions (Invitrogen). RNA concentration was measured by Nanodrop (ThermoFisher Scientific) and RNA was stored at -20ºC. RNA quality was determined by spectrophotometry (Nanodrop) and by Bioanalyser (Ramaciotti Centre for Gene Function Analysis, University of New South Wales, Australia). Preparation of cRNA, probes, and hybridization to whole yeast genome microarrays (YG-S98, Affymetrix) was performed at the Ramaciotti Centre. Candidate differentially expressed genes with a significant Bonferroni adjusted p value < 0.05 and fold-change > 2.0 (mutant versus WT) were identified using *limma* R package (21) after normalization by robust-multiarray average (MRA) algorithm from *affy* R package (22).

Rate of CoQ_6 synthesis

For determination of CoQ_6 synthesis rates, WT and *cho2Δ* cells were grown in SD-4HB-pABA (30 °C shaking) until OD_{600} ~0.5 and then either $^{13}C_6$-4-hydroxybenzoic acid (Cambridge isotope, USA) or unlabelled 4-hydroxybenzoic acid was added to a final concentration of 200 μg. Cell were harvested at OD_{600} ~1.0 and 2.0 and cell pellets were store at -20 °C until analyses. On the day of analysis, cells were defrosted and CoQ_6 and $^{13}CoQ_6$ were extracted from yeast cells using acidified methanol and hexane as described above and 2 μL injected onto an Agilent 1290 UHPLC system connected to an Agilent 6490 triple-quadrupole mass spectrometer with column, mobile phases, gradient elution, flow rate and mass spectrometry parameters as above. MRM settings for $^{13}C_6$-CoQ_6 (parent ion→fragment ion) were *m/z*

597.3→ 203.1 with collision energy (CE) = 33 V. $^{13}C_6$-CoQ_6 was quantified against authentic CoQ_6 commercial standard and rate of synthesis determined.

CoQ_6 content in yeast mitochondria

Yeast cultures of WT BY4743 and *cho2Δ* were grown overnight. Pre-cultures were diluted and grown overnight with shaking (30 °C) until cell density reached OD_{600} ~1.0. Spheroplasts were prepared with Zymolyase-20T (MP Biomedicals) and fractionated as previously described (23) in the presence of cOmplete™ EDTA-free protease inhibitor cocktail tablets (Roche), phosphatase inhibitor cocktail set I (Sigma-Aldrich), phosphatase inhibitor cocktail set II (Sigma-Aldrich) and phenylmethylsulfonyl fluoride (PMSF). Purified mitochondria were frozen in liquid nitrogen, aliquoted, and stored at -80 °C until analyses. Protein concentration of mitochondria was measured by the bicinchoninic acid (BCA) assay (ThermoFisher Scientific). On the day of analysis, mitochondrial extracts were defrosted, and lipid extracted in the presence of internal standard CoQ_4 and analyzed for CoQ_6 by LC-MS/MS as previously described (16).

Mitochondrial DNA determination

Mitochondrial DNA estimation was carried out as previously described (3). Briefly, yeast cells at OD_{600} ~1.0 were collected by centrifugation at 3000 x *g* for 5 min, washed with H_2O, and frozen at -20 °C until DNA extraction was carried out. Cell pellets were resuspended in 200 µL lysis buffer (10 mM Tris-Cl pH 8.0, 2% (v/v) Triton X-100, 1 mM EDTA, 100 mM NaCl, 1% SDS), and 200 µL acid-washed glass beads and 200 µL of phenol:chloroform:isoamyl alcohol (25:24:1) were added to the cell suspension. Cells were lysed using a bead-beater (Precellys 24; Bertin Technologies) for 3 x 10 s at 6500 rpm with a 45 s break between rounds at 4ºC. 200 µL of Tris-EDTA (TE) buffer (10 mM Tris-Cl, 1 mM EDTA) was added and cell suspension was centrifuged at 13,000 x *g* for 5 min at room temperature. The aqueous layer was removed to a new tube containing 200 µL of chloroform, mixed by inversion and centrifuged at 13,000 x *g* for 5 min at room temperature. This was repeated once more. After this, the aqueous layer was transferred to a 2 mL screw-cap tube containing 1 mL of 95% ethanol, mixed by inversion, and centrifuged at 13,000 x *g* for 2 min at room temperature. The resulting pellet was resuspended in 400 µL of TE containing 30 µg RNase A and incubated at 37ºC for 30 min. 10 µL of 3 M sodium acetate and 1 mL of 95% ethanol was added, mixed by inversion, and incubated at -20ºC for 1 h. After 1 h of incubation at -20ºC, the suspension was centrifuged at 13,000 x *g* for 5 min and the pellet washed twice with 70% v/v ethanol and air dried. The dried pellet was resuspended in 25 µL of TE and concentration measured by Nanodrop (ThermoFisher Scientific) and stored at -20 °C until use.

qPCR was performed on a CFX384 instrument (Bio-Rad) using the SensiFAST™ SYBR® No-ROX kit (Bioline) as per the manufacturer's instructions. Each sample was run in duplicate with 150 ng of total DNA used per reaction using the following thermocycling protocol (95 °C for 2 min, 95 °C for 5 s, 60 °C for 10 s, and 72 °C for 20 s, plate read and cycle repeated X40, melt curve 40 –92 °C with plate read and 40 °C for 10 s). Melting curve analysis confirmed that all PCRs produced a single product. mtDNA-specific primers and actin-specific primers were used (see Table S3 for primers mtDNA_F, mtDNA_R, ACT1F and ACTR*).* The relative level of gene expression of mitochondrial DNA was normalised to the level of actin as described previously (24).

Citrate synthase activity

The measurement of citrate synthase activity in yeast cells was carried out as described previously (25). Briefly, yeast cells at approximately OD_{600} ~1.0 were collected by centrifugation at 3,000 x *g* for 5 min, washed with H_2O, and frozen at -20 °C until activity assays were carried out. On the day of analysis, cell pellets were defrosted and resuspended in 200 µL lysis buffer (100 mM Tris-Cl pH 7.4, 1% (v/v) Triton X-100, 1 mM EDTA, 1 mM phenylmethylsulfonyl fluoride, 1 x cOmplete™ Protease Inhibitor Cocktail (Roche)), with 200 µL acid-washed glass beads. Cells were lysed using a bead-beater (Precellys 24; Bertin Technologies) for 3 x 10 s at 6500 rpm with a 45 s break between rounds at 4 °C. The clarified cell lysate was collected after centrifugation at 16,000 x *g* for 10 min at 4 °C. Bicinchoninic acid assay (ThermoFischer Scientific) was done to quantify the protein concentration. Cell lysates were normalized to 0.05 µg/uL protein. The citrate synthase assay was carried out using a VersaMax plate reader (Molecular Devices) in a flat-bottom 96 well plate. 40 µL of 500 mM Tris-Cl pH 7.4, 2 µL of 30 mM acetyl CoA, 8 µL of 2.5 mM 5,5'- dithio-*bis*(2-nitrobenzoic acid) (DTNB), 90 µL H_2O, and 50 µL cell lysate (2.5 µg total protein), were added into each well. 10 µL of 10 mM oxaloacetic acid was added per well and mixed by pipetting up and down. Absorbance at 412 nm (A_{412}) was measured every 30 s at 25 °C. The initial slope was calculated by using data from the first 10 min and used to determine the enzyme reaction rate using the extinction coefficient for TNB of 14.15 mM^{-1} cm^{-1} (26).

Quantitative real-time PCR (qRT-PCR)

Total RNA was isolated from cells or tissue using TRIzol reagent (Invitrogen). For yeast RNA, DNA contamination was removed using the DNase TURBO kit as per manufacturer's instructions (Invitrogen). RNA concentration was measured by Nanodrop (ThermoFisher Scientific) and RNA was stored at -20 °C. Reverse transcription was carried out using the Superscript III first strand synthesis system using random hexamer primers (Invitrogen). cDNA was stored at -20 °C until qPCR analyses were carried out. Quantitative real-time PCR was

performed on a CFX384 instrument (BioRad) using the SensiFAST™ SYBR® No-ROX kit (Bioline) in duplicate. The relative levels of gene expression were normalized to the expression level of actin or cyclophilin D as indicated. Melting curve analysis confirmed that all PCR reactions produced a single product. The primers (forward/reverse) used in real-time PCR were designed using Primer3 online (http://bioinfo.ut.ee/primer3/) for yeast primers or the PrimerBank database (https://pga.mgh.harvard.edu/primerbank/index.html) for mouse primers. All primers used are listed in Table S3.

Determination oxygen consumption in yeast cells using high-resolution respirometry

High resolution respirometry to determine basal and maximal oxygen consumption rates was carried out using an Oroboros O2k Oxygraph system. WT and *cho2*Δ yeast cells were grown until OD_{600} ~1.0. 1 OD of cells were harvested by centrifugation (17,000 x *g*; 10 min; 4 °C) and resuspended in 6 mL of fresh medium. Each chamber of the Oroboros O2k Oxygraph was filled with 3 mL of cell suspension and the stoppers carefully inserted to ensure no air bubbles remained in the chamber. Routine/basal respiration was acquired by allowing the cells to equilibrate in the chambers until a steady reading was reached and oxygen consumption recorded. Mitochondrial membrane potential was then collapsed to acquire maximal flux through the electron transfer system by three sequential addition of 10 mM 2-[[4-(trifluoromethoxy)phenyl]hydrazinylidene]propanedinitrile (FCCP). Residual oxygen flux was then acquired by the addition of 1 M sodium azide. Each sample was measured in technical duplicate.

SDS-PAGE and immunoblot analysis

Whole cell immunoblot - Briefly, yeast cells at OD_{600} ~1.0 were collected by centrifugation at 3000 x *g* for 5 min, washed with H_2O, and frozen at -20 °C until protein extraction was carried out. For protein extraction, cell pellets were resuspended in Thorner buffer (40 mM Tris-Cl pH 8.0, 5% w/v SDS, 8 M urea, 100 µM EDTA, 1 mM phenylmethylsulfonyl fluoride, 1 x cOmplete™ Protease Inhibitor Cocktail (Roche)), and 200 µL acid-washed glass beads were added. Cells were lysed using a bead-beater (Precellys 24; Bertin Technologies) for 3 x 10 s at 6500 rpm with a 45 s break between rounds at 4 °C. The clarified cell lysate was collected after centrifugation at 17,000 x *g* for 10 min at 4 °C. BCA assay (ThermoFischer Scientific) was done to quantify protein concentration. 20 µg of protein were resuspended in SDS sample buffer (50 mM Tris-Cl pH 6.8, 2% w/v SDS, 0.1% bromophenol blue, 10% (v/v) glycerol, 100 mM DTT) and separated by SDS gel electrophoresis on 10% NuPAGE Bis-Tris gels (Thermo Fischer Scientific) using MOPS running buffer (50 mM MOPS, 50 mM Tris Base, 0.1% SDS, 1 mM EDTA pH 7.7). Proteins were transferred to nitrocellulose membrane using the iBlot2 system (Thermo Fischer Scientific) using Program 0 and then blocked using 10% skim milk

and 0.05% Triton X-100 in Tris-buffered saline for 1 h at room temperature. Porin and actin (antibody dilutions in Table S4) were probed with mouse monoclonal antibodies prepared in 5% skim milk and 0.05% Triton X-100 in Tris-buffered saline overnight at 4 °C. Anti-mouse IgG secondary antibody (Dako) was used at dilution of 1:10,000 in 5% skim milk and 0.05% Triton X-100 in Tris-buffered saline for 1 h at room temperature. Proteins were visualized on film using chemiluminescent detection. Immunoblots are representative of six replicates and were quantified by hand using ImageStudio Lite software with porin content normalized to actin.

Isolated mitochondria immunoblot—Purified mitochondria (25 μg) were resuspended in SDS sample buffer and separated by SDS gel electrophoresis on 10% or 12% Tris-glycine polyacrylamide gels. Proteins were transferred to 0.45 μm PVDF membrane (Millipore) and blocked with blocking buffer (0.5% BSA, 0.1% Tween 20, 0.02% SDS in phosphate-buffered saline). Representative Coq polypeptides and loading control mitochondrial malate dehydrogenase (Mdh1) were probed with rabbit polyclonal antibodies prepared in blocking buffer at dilutions listed in Table S4. IRDye 680LT goat anti-rabbit IgG secondary antibody (LiCOR) was used at a dilution of 1:10,000. Proteins were visualized using a LiCOR Odyssey Infrared Scanner (LiCOR). Immunoblots are representative of three replicates and were quantified by hand using ImageStudioLite software normalized to Mdh1.

Two-dimensional Blue Native/SDS-PAGE immunoblot analysis of high molecular weight complexes

Two-dimensional Blue Native (BN)/SDS-PAGE was performed as described (27-29). Briefly, 200 μg of purified mitochondria were solubilized at 4 mg/mL for one hour on ice with 16 mg/mL digitonin (Biosynth) in the presence of the protease and phosphatase inhibitors used during mitochondrial isolation. Protein concentration of solubilized mitochondria was determined by BCA assay. NativePAGE 5% G-250 sample additive (ThermoFisher Scientific) was added to a final concentration of 0.25%. 80 μg of solubilized mitochondria were separated on NativePAGE 4-16% Bis-Tris gels (ThermoFisher Scientific) in the first dimension, and native gel slices were further separated on 12% Tris-glycine polyacrylamide gel in the second dimension. Following the second-dimension separation, immunoblot analyses were performed as described above, using antibodies against Coq4 at the dilutions indicated in Table S4. Molecular weight standards for BN gel electrophoresis and SDS gel electrophoresis were obtained from GE Healthcare (Sigma-Aldrich) and Bio-Rad, respectively

Phosphatidylcholine, dolichol and triacylglyceride extraction from yeast cells

100 μL of 50% methanol containing 100 μM DTPA was added to harvested cell pellets and barocycled at 40 kpsi (50 s on, 10 s off for 30 cycles at 20 °C) using a Barocycler 2320EXT

(Pressure BioSciences Inc). Cell lysates were transferred to microcentrifuge tubes and 50 µL butylated hydroxytoluene, 2.5 µL internal standard diluted in methanol (SPLASH® LIPIDOMIX® Mass Spec Standard; Sigma-Aldrich), 380 µL 50% methanol and 250 µL chloroform added. Samples were vortexed vigorously for 1 min at room temperature and then centrifuged at 17,000 x *g* for 10 min at 4 °C. 200 µL of chloroform was removed and transferred to an LC/MS vial. 250 µL of chloroform added to the sample, vortexed vigorously for 1 min at room temperature and then centrifuged at 17,000 x *g* for 10 min at 4 °C. 250 µL of chloroform was removed and combined with the first 200 µL aliquot removed. Chloroform was dried under nitrogen and dried lipids were stored at -80 °C until analyses. Prior to analyses, dried lipids were resuspended in 100 µL of chloroform:methanol (1:1, vol:vol) and subjected to LC/MS analysis as outlined below.

Lipid analyses by LC-MS/MS

Lipid analysis of yeast extracts was performed as described previously (30) using an Agilent 6560 Ion Mobility Q-TOF LC/MS coupled to a 1290 Infinity II UPLC system. Lipids were separated on Waters Acquity CSH C18 column (1.7 µm, 100 mm x 2.1 mm). 5 µL of lipid extract was subjected for LC/MS analysis. Column was kept at 55 °C and elution gradient consisted of mobile phase A (water/acetonitrile, 4:6, v/v) with 10 mM ammonium formate and mobile phase B (acetonitrile/2-propanol, 1:9, v/v) with 10 mM ammonium formate. The flow rate was 0.3 mL/min and the gradient ran from 0 to 40% mobile phase B in the first 6 min, increased to 100% mobile phase B in the next 24 min, kept at 100% mobile phase B for further 4 min, and returned to 0% mobile phase B over 2 min followed by column equilibration for another 4 min (total run time of 40 min). Lipids were analyzed in positive ionization polarity mode with electrospray settings as follows: gas temperature 300 °C, drying gas flow 5 L/min, sheath gas temperature 300 °C; sheath gas flow 12 L/min; cap voltage 3.5 kV. Auto MS/MS mode was used to acquire data with scan range of 100-1700 m/z and collision energy 35 eV. M/z 121.0509 and m/z 922.0098 ions were used as "lock masses" and were introduced by constant infusion of reference calibration solution. Peak detection and peak area integration were performed using Mass Hunter Workstation Software (Agilent Technologies, USA). Identification of lipid species were performed using acquired MS/MS data and LipidMatch software (31).

MitoSOX measurements

Yeast cells at OD_{600} ~1.0 were collected by centrifugation at 3000 x *g* for 1 min, washed with phosphate buffered saline (PBS) twice and resuspended in PBS for a final concentration of 1 OD unit. MitoSOX was added to the yeast suspension (5 µM end concentration; 50 µM stock made in PBS). Cells were incubated in the dark at 30 °C for 45 min with gentle shaking. After

45 min, cells were washed twice in PBS, resuspend in fresh PBS and pipetted into a black multi-well plate. Fluorescent was measured using a PHERAStar FSX (BMG Lab Tech) with a 510/580 nm (ex/em) detector as per Manufacturer's instructions.

Fatty acid sensitivity assay

Sensitivity of yeast cells to PUFA-induced oxidative stress was performed as described previously (3). Briefly, cells were grown overnight at 30 °C shaking. Cultures were sub-inoculated to an OD_{600}= 0.25 in fresh medium and incubated at 30 °C, shaking until cells reached OD_{600} ~1.0. Cells were harvested, washed twice with sterile water, and diluted in 0.1 M phosphate buffer with 0.2% dextrose, pH 6.2, to an OD_{600} = 0.2. The cell suspension was divided into 5-ml aliquots and treated with an ethanol vehicle control (final concentration 0.1% v/v), ethanol-diluted oleic acid (Nu-Check Prep), or α-linolenic acid (Nu-Check Prep) to a final concentration of 200 µM. Fatty acid-treated cultures were incubated for 4 h at 30 °C shaking, after which cell viability was assessed via plate dilutions. Cell viability prior to the addition of fatty acids was determined via plate dilutions, represented in the 0-h plate.

PEMT knockdown in 3T3-L1 adipocyte via anti-sense oligonucleotide (ASO) treatment

At 6-7 days post differentiation, 3T3-L1 adipocytes were transfected with control scrambled and anti-PEMT antisense oligonucleotides (ASO; Ionis Pharmaceuticals Inc.) as per *in vivo* mouse studies. To transfect cells, 300 nmol ASO, 7.5 µL Trans-ITX2 Dynamic delivery system and 100 µL of OptiMEM (per 12-well) were combined and incubated at room temperature for 30 min. During this incubation time, 3T3-L1 adipocytes were trypsinized (5x trypsin, EDTA; Thermo Fisher Scientific) at 37°C and centrifuged at 120 x *g* for 5 min at room temperature. Adipocytes were resuspended in DMEM/10% FCS/GlutaMAX and the appropriate ASO-solution added. Cells were seeded onto Matrigel (Corning) coated plates and grown for 4 d. Pemt knockdown by ASO treatment was verified using qPCR.

TNFα treatment of in 3T3-L1 adipocytes

Insulin resistance was induced by tumor necrosis factor-α (TNFα) in 3T3-L1 adipocytes as previously described (32). At 6-7 days post differentiation, 3T3-L1 adipocytes were incubated with 2 ng/mL TNFα (R&D Systems) diluted in phosphate buffered saline for 4 d. Medium was changed every 24 h and replaced with fresh medium containing 2 ng/mL TNFα.

CoQ synthesis inhibition in 3T3-L1 adipocytes

At 6-7 days post differentiation, 3T3-L1 adipocytes were treated with 1 mM 4-nitrobenzoic acid made in DMEM/10% FCS/GlutaMAX to inhibit CoQ synthesis (33). Medium was changed every 24 h and replaced with fresh medium containing 1 mM 4-nitrobenzoic acid.

2-Deoxyglucose (2-DOG) uptake assays in cultured cells

2-Deoxyglucose (2-DOG) uptake was measured as previously described (7). 3T3-L1 cells were differentiated and grown as outlined above in 24-well plates. To measure 2-DOG uptake, cells were serum starved for 2 h in DMEM/0.2% BSA/1% GlutaMAX at 37ºC/5% CO_2. Cells were washed and incubated in pre-warmed (37ºC) Krebs–Ringer phosphate (KRP) buffer (0.6 mM Na_2HPO_4, 0.4 mM NaH_2PO_4, 120 mM NaCl, 6 mM KCl, 1mM $CaCl_2$, 1.2 mM $MgSO_4$ and 12.5 mM HEPES (pH 7.4) containing 0.2% bovine serum albumin and 24-well plates transferred to a 37 ºC water bath for the assay. Cells were stimulated with 100 nM insulin for 20 min and 25 mM cytochalasin B (Sigma Aldrich) was added as a control to determine non-specific 2-DOG uptake to the wells before addition of 2-[^{3}H]deoxyglucose (PerkinElmer). During the final five min, tritiated 2-DOG (0.025 mCi, 50 mM) was added to cells to measure steady-state rates of labelled 2-DOG uptake. Following three washes with ice-cold PBS, cells were solubilized in PBS containing 1% (v/v) Triton X-100. Tracer uptake was quantified by liquid scintillation counting (Packard Tri-Carb β-scintillation counter using Optima XR scintillation fluid, Perkin Elmer). Samples were read for 5 min and Disintegrations Per Minute (DPM) used for data analysis. Data was normalized for protein content and further normalized to Δ glucose uptake (insulin treated minus control values).

Statistical analyses

All statistical analyses were carried out using GraphPad Prism V8.

References

1. Brachmann CB, Davies A, Cost GJ et al. Designer deletion strains derived from *Saccharomyces cerevisiae* S288C: a useful set of strains and plasmids for PCR-mediated gene disruption and other applications. *Yeast* 1998;14:115-32.
2. Winzeler EA, Shoemaker DD, Astromoff A et al. Functional characterization of the *S. cerevisiae* genome by gene deletion and parallel analysis. *Science* 1999;285:901-6.
3. Bradley MC, Yang K, Fernández-Del-Río L et al. *COQ11* deletion mitigates respiratory deficiency caused by mutations in the gene encoding the coenzyme Q chaperone protein Coq10. *J. Biol. Chem.* 2020;295:6023-42.
4. *Saccharomyces* Genome Deletion Project Consortium. http://www-sequence.stanford.edu/group/yeast_deletion_project/deletions3.html 2007.
5. Santos JH, Mandavilli BS, Van Houten B. Measuring oxidative mtDNA damage and repair using quantitative PCR. *Methods Mol. Biol.* 2002;197:159-76.
6. Croft KD, Zhang D, Jiang R et al. Structural requirements of flavonoids to induce heme oxygenase-1 expression. *Free Radic. Biol. Med.* 2017;113:165-75.
7. Fazakerley DJ, Chaudhuri R, Yang P et al. Mitochondrial CoQ deficiency is a common driver of mitochondrial oxidants and insulin resistance. *eLife* 2018;7:e32111.
8. Gin P, Clarke CF. Genetic evidence for a multi-subunit complex in coenzyme Q biosynthesis in yeast and the role of the Coq1 hexaprenyl diphosphate synthase. *J. Biol. Chem.* 2005;280:2676-81.
9. Hsieh EJ, Gin P, Gulmezian M et al. *Saccharomyces cerevisiae* Coq9 polypeptide is a subunit of the mitochondrial coenzyme Q biosynthetic complex. *Arch. Biochem. Biophys.* 2007;463:19-26.
10. Poon WW, Barkovich RJ, Hsu AY et al. Yeast and rat Coq3 and *Escherichia coli* UbiG polypeptides catalyze both *O*-methyltransferase steps in coenzyme Q biosynthesis. *J. Biol. Chem.* 1999;274:21665-72.
11. Belogrudov GI, Lee PT, Jonassen T, Hsu AY, Gin P, Clarke CF. Yeast *COQ4* encodes a mitochondrial protein required for coenzyme Q synthesis. *Arch. Biochem. Biophys.* 2001;392:48-58.
12. Baba SW, Belogrudov GI, Lee JC et al. Yeast Coq5 C-methyltransferase is required for stability of other polypeptides involved in coenzyme Q biosynthesis. *J. Biol. Chem.* 2004;279:10052-9.
13. Gin P, Hsu AY, Rothman SC et al. The *Saccharomyces cerevisiae COQ6* gene encodes a mitochondrial flavin-dependent monooxygenase required for coenzyme Q biosynthesis. *J. Biol. Chem.* 2003;278:25308-16.
14. Tran UC, Marbois B, Gin P, Gulmezian M, Jonassen T, Clarke CF. Complementation of *Saccharomyces cerevisiae coq7* mutants by mitochondrial targeting of the *Escherichia coli* UbiF polypeptide: two functions of yeast Coq7 polypeptide in coenzyme Q biosynthesis. *J. Biol. Chem.* 2006;281:16401-9.
15. Wang Y, Luo L, Braun OÖ et al. Neutrophil extracellular trap-microparticle complexes enhance thrombin generation via the intrinsic pathway of coagulation in mice. *Sci. Rep.* 2018;8:4020.
16. Tsui HS, Pham NVB, Amer BR et al. Human $COQ_{10}A$ and $COQ_{10}B$ are distinct lipid-binding START domain proteins required for coenzyme Q function. *J. Lipid Res.* 2019;60:1293-310.
17. Sprague GF, Jr. Assay of yeast mating reaction. *Methods Enzymol.* 1991;194:77-93.
18. Janke C, Magiera MM, Rathfelder N et al. A versatile toolbox for PCR-based tagging of yeast genes: new fluorescent proteins, more markers and promoter substitution cassettes. *Yeast* 2004;21:947-62.
19. Gietz RD, Woods RA. Transformation of yeast by lithium acetate/single-stranded carrier DNA/polyethylene glycol method. *Methods Enzymol.* 2002;350:87-96.

20. Marobbio CM, Agrimi G, Lasorsa FM, Palmieri F. Identification and functional reconstitution of yeast mitochondrial carrier for *S*-adenosylmethionine. *EMBO J.* 2003;22:5975-82.

21. Ritchie ME, Phipson B, Wu D et al. limma powers differential expression analyses for RNA-sequencing and microarray studies. *Nucleic Acids Res.* 2015;43:e47.

22. Gautier L, Cope L, Bolstad BM, Irizarry RA. affy--analysis of Affymetrix GeneChip data at the probe level. *Bioinformatics* 2004;20:307-15.

23. Glick BS, Pon LA. Isolation of highly purified mitochondria from *Saccharomyces cerevisiae. Methods Enzymol.* 1995;260:213-23.

24. Gonzalez-Hunt CP, Rooney JP, Ryde IT, Anbalagan C, Joglekar R, Meyer JN. PCR-based analysis of mitochondrial DNA copy number, mitochondrial DNA damage, and nuclear DNA damage. *Curr. Protoc. Toxicol.* 2016;67:20.11.1-20.11.25.

25. Guo X, Niemi NM, Hutchins PD et al. Ptc7p dephosphorylates select mitochondrial proteins to enhance metabolic function. *Cell Rep.* 2017;18:307-13.

26. Eyer P, Worek F, Kiderlen D et al. Molar absorption coefficients for the reduced Ellman reagent: reassessment. *Anal. Biochem.* 2003;312:224-7.

27. He CH, Xie LX, Allan CM, Tran UC, Clarke CF. Coenzyme Q supplementation or overexpression of the yeast Coq8 putative kinase stabilizes multi-subunit Coq polypeptide complexes in yeast coq null mutants. *Biochim. Biophys. Acta*. 2014;1841: 630-644

28. Schägger H, Cramer WA, von Jagow G. Analysis of molecular masses and oligomeric states of protein complexes by blue native electrophoresis and isolation of membrane protein complexes by two-dimensional native electrophoresis. *Anal. Biochem*. 1994;217: 220-230

29. Wittig, I, Braun HP, Schägger H. Blue NativePAGE. *Nat. Protoc*. 2006;1: 418-428

30. Ackerman D, Tumanov S, Qiu B et al. Triglycerides promote lipid homeostasis during hypoxic stress by balancing fatty acid saturation. *Cell Rep.* 2018;24:2596-605.

31. Wang C, Cheng D, Jalali Motlagh N et al. Highly efficient activatable MRI probe to sense myeloperoxidase activity. *J. Med. Chem.* 2021;64:5874-85.

32. Hoehn KL, Hohnen-Behrens C, Cederberg A et al. IRS1-independent defects define major nodes of insulin resistance. *Cell Metab.* 2008;7:421-33.

33. Forsman U, Sjöberg M, Turunen M, Sindelar PJ. 4-Nitrobenzoate inhibits coenzyme Q biosynthesis in mammalian cell cultures. *Nat. Chem. Biol.* 2010;6:515-7.